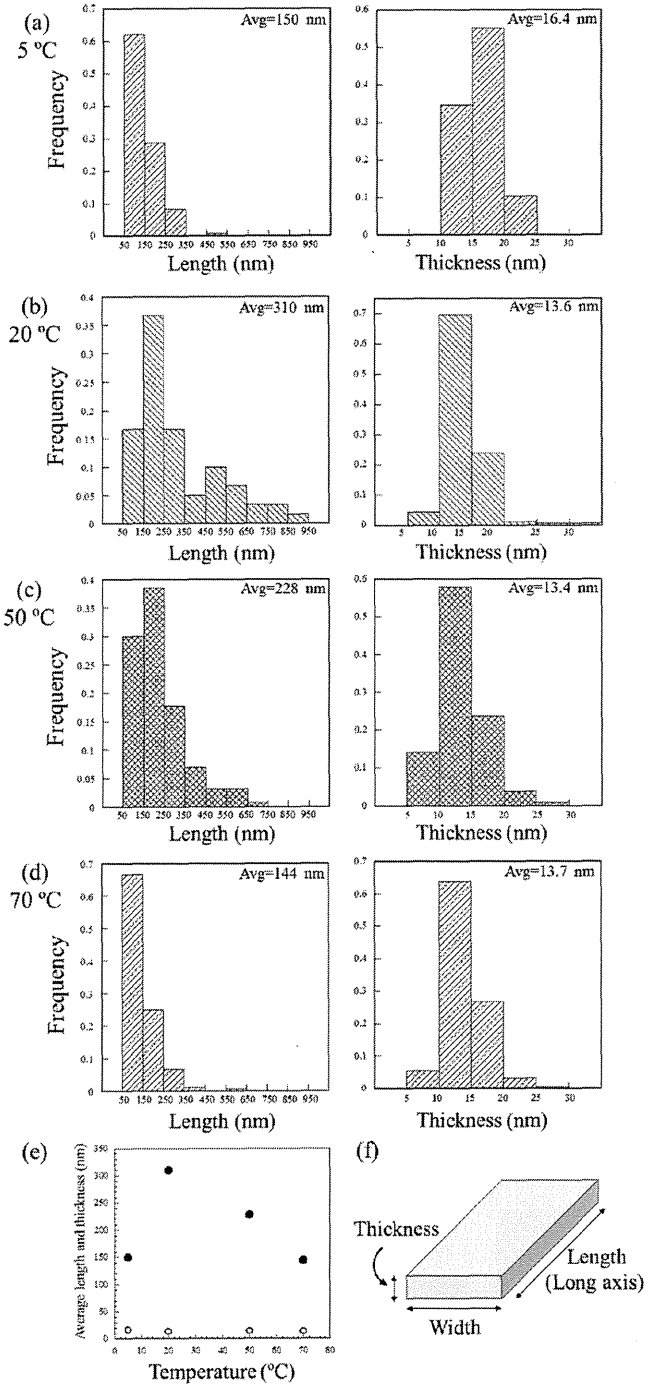

Figure 6. Size distribution histograms of a dispersion of GG-236MC (**2**, 0.2 wt %) in water obtained by measuring the length and thickness on cryo-TEM micrographs at (a) 5, (b) 20, (c) 50, and (d) 70 °C. (e) Average length and thickness vs temperature: (●) length and (○) thickness. (f) Schematic representation of the ribbonlike nanostructure.

larger with increasing temperature from 5 to 20 °C, indicating the growth of ribbonlike nanostructures along the axis. With increasing temperature from 20 to 70 °C, the length of the ribbonlike nanostructures decreased in the direction of the long axis.

It was found that diblock MCs with different DP values showed different temperature-dependent behaviors, even if the DS values of diblock MCs were almost the same. G-236MC (**1**, DP_n = 10.7 and DS = 2.65) having fewer than ten 2,3,6-tri-*O*-methyl-glucopyranosyl units exhibited no gelation as recently reported. This was likely because G-236MC (**1**) formed disklike and multilamellar nanostructures rather than ribbonlike nanostructures.

SAXS Measurements of GG-236MC (2). A dispersion of GG-236MC (**2**, DP_n = 28.2 and DS = 2.75) was investigated by SAXS measurements to obtain more precise information on the structure and dimensions of the nanostructures. Figure 7 shows the diffractograms obtained for a dispersion of GG-236MC (**2**, 0.2 wt %) in water at 5, 30, 50, and 70 °C. According to the analysis by NANOFIT software, the scattering curves were well fitted to the cylinder model with a short height, that is, the disklike model. The radii of the cylinders were 19.5, 16.8, 18.4, and 17.5 nm at 5, 30, 50, and 70 °C, respectively, as shown in Figure 7b. The radii were in good agreement with the molecular length (ca. 14 nm) of GG-236MC (**2**) calculated from DP_n = 28.2. Furthermore, at increasing temperature from 5 to 30 °C, the height of the cylinder increased from 2.1 to 3.4 nm and remained constant (6.3 nm) above 50 °C (Figure 7b).

The results from NANOFIT analysis suggested the following temperature-dependent self-assembled ribbonlike nanostructures. The SAXS experiments suggested that GG-236MC molecules (**2**) were oriented perpendicular to the long axis of ribbonlike nanostructure with bilayer structure having a width of ca. 40 nm. The cylinder model having a height of 2–6 nm was stacked horizontally with respect to the thickness direction of ribbonlike nanostructures, though the average thickness of ribbonlike nanostructures from cryo-TEM micrographs was ca. 14 nm. At 5 °C, the ribbonlike nanostructures consisted of the periodic diffraction structure having a height of 2 nm in the thickness direction as a result of the loose packing between molecules. At 30 °C, the height of the periodic structure increased to 3.4 nm as dehydration proceeded. Above 50 °C, the periodic height remained constant (6.3 nm) likely because of the dehydration between GG-236MC (**2**) molecules.

WAXS Measurement of GG-236MC (2). The crystalline morphology of the 2.0 wt % gel of GG-236MC (**2**, DP_n = 28.2 and DS = 2.75) was investigated at approximately 15 °C by WAXS measurement. The diffraction patterns of (a) 2,3,6-tri-*O*-methylcellulose (powder sample, DP_n = 201, M_w/M_n = 2.71), (b) a 2.0 wt % gel of GG-236MC (**2**), and (c) the dried sample prepared from a 2.0 wt % gel of GG-236MC (**2**) are shown in Figure 8. The diffractogram of (a) 2,3,6-tri-*O*-methyl-cellulose showed diffraction peaks at 2θ = 7.6 and 19.9. The diffraction peaks of (b) the gel and (c) the dried sample of GG-236MC (**2**) coincided well with those of (a) 2,3,6-tri-*O*-methyl-cellulose. The crystal lattice of GG-236MC (**2**) would be same as that of 2,3,6-tri-*O*-methyl-cellulose because GG-236MC (**2**) had a segment consisting of approximately twenty-seven 2,3,6-tri-*O*-methyl-glucopyranosyl units. Zugenmaier et al. have concluded from X-ray and electron diffraction data that the crystal structure of 2,3,6-tri-*O*-methylcellulose was regarded as orthorhombic with four chains running through the unit cell and axis values of a = 0.46 nm, b = 4.32 nm, and c = 1.04 nm (fiber axis).[32] Furthermore, two pairs of parallel chains of 2,3,6-tri-*O*-methyl-cellulose were packed in an antiparallel fashion because only chains running antiparallel have been detected in single crystals grown from solutions. There have been some reports on the WAXS measurement of commercial MC in the gel state.[8,33] Kato et al. have reported that the peak position of the X-ray diffraction pattern of the MC gel coincided well with those of 2,3,6-tri-O-methylcellulose, indicating that the cross-

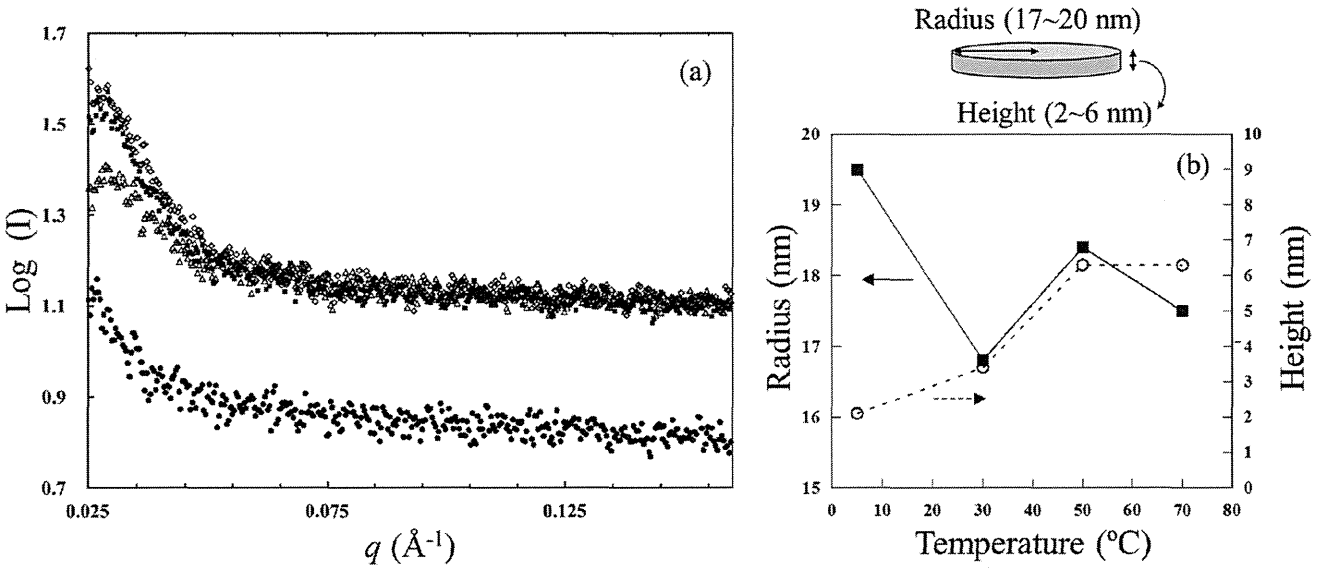

Figure 7. (a) Scattering intensity as a function of the scattering vector for a dispersion of GG-236MC (**2**, 0.2 wt %) in water at increasing temperature: (●) 5, (△) 30, (■) 50, and (◊) 70 °C. (b) Radius of the nanostructure obtained by NANOFIT software using the cylinder model as a function of temperature for a dispersion of GG-236MC (**2**, 0.2 wt %).

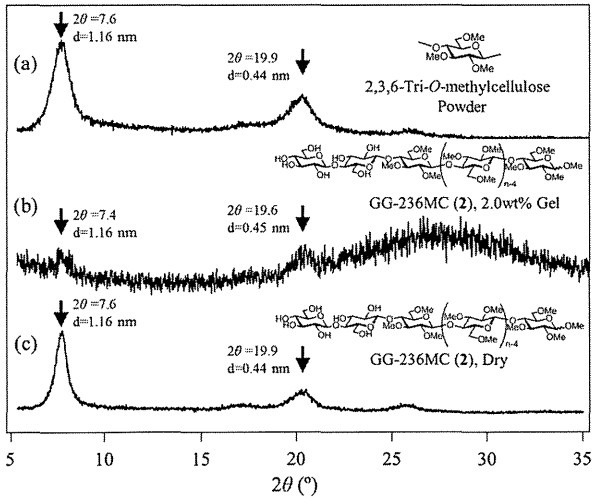

Figure 8. Wide angle X-ray diffractograms of (a) 2,3,6-tri-*O*-methylcellulose, (b) GG-236MC (**2**), a 2.0 wt % gel sample, and (c) GG-236MC (**2**), a dried sample.

linking loci of MC gels consists of crystallites of 2,3,6-tri-*O*-methyl-glucopyranose sequences.[8] However, the gel structure and gelation mechanism of MC are still uncertain because commercial MC has a heterogeneous structure. In summary, the WAXS measurement of GG-236MC (**2**) having a well-defined structure strongly suggested that the gelation of GG-236MC (**2**) was attributed to the close packing between the sequences of 2,3,6-tri-*O*-methyl-glucopyranose units. This intermolecular interaction was of fundamental significance not only for the gelation of commercial MC[8] but also for that of present real diblock MC (**2**, DP_n = 28.2 and DS = 2.75).

Possible Mechanism for the Self-Assembly and Gelation of G-236MC (1) and GG-236MC (2). On the basis of the results from cryo-TEM, SAXS, and WAXS, the self-assembling mechanism of diblock copolymers G-236MC (**1**, DP_n = 10.7 and DS = 2.65) and GG-236MC (**2**, DP_n = 28.2 and DS = 2.75) is illustrated in Figure 9.

At 5 °C, G-236MC (**1**) dissolved well and was hydrated, whereas GG-236MC (**2**) was dispersed in water and formed self-assembled nanostructures. As the temperature increases, the surrounding water molecules near the diblock copolymer are detached, resulting in the diblock copolymers being dehydrated to form the crystalline regions consisting of the sequences of 2,3,6-tri-*O*-methyl-glucopyranosyl units. The WAXS measurement suggested the presence of these crystalline regions in the gel state. The endothermic peak of the dehydration phenomena has been detected in the DSC curve at around 30 °C.[21] The DSC studies on the endothermic dehydration phenomenon of commercial MC have been reported by many researchers.[9,17,29,34−36] However, there has been no consensus on the dehydration at the endothermic peak temperature. In contrast, DSC measurements of GG-236MC (**2**) in combination with cryo-TEM, SAXS, and WAXS measurements strongly suggested that the dehydration occurred at 30 °C because of the hydrophobic interaction between the sequences of 2,3,6-tri-*O*-methyl-glucopyranosyl units. At around 30 °C, the formation and growth of crystalline regions accompanied by the expulsion of water molecules and the entanglement of ribbonlike nanostructures accompanied by the entrapment of water occurred almost simultaneously. GG-236MC (**2**, DP_n = 28.2 and DS = 2.75) formed a hydrogel at 2.0 wt % concentration at 25 °C within 1 h. This fact indicated the formation of self-assembled nanostructures below endothermic temperature at approximately 30 °C at a heating rate of 3.5 °C/min in the DSC curve. Note that this gelation behavior at temperature lower than the dehydration temperature detected by DSC is similar to that of MC reported by Joshi et al.[37] Thus, we concluded that the difference between cryo-TEM and DSC attributed to their thermal history. The diblock copolymers self-assemble in water, resulting in the formation of ribbonlike supramolecular nanostructures by hydrophobic interaction between the sequence of 2,3,6-tri-*O*-methyl-glucopyranosyl units. The formation of hydrophobic environments of self-assembled nanostructures has been analyzed by a fluorescent probe method.[21] Further increases in temperature cause the growth of nanostructures.

dx.doi.org/10.1021/la3026528 | *Langmuir* 2012, 28, 12609−12618

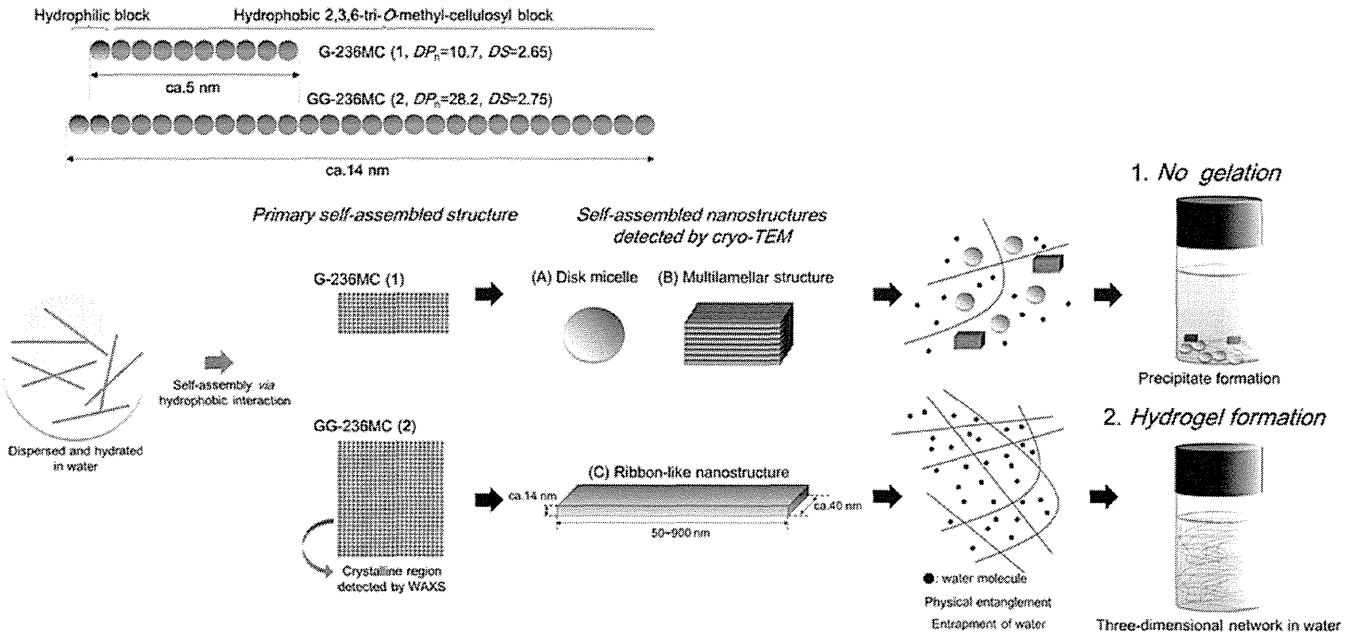

Figure 9. Schematic representation of the possible gelation mechanism of G-236MC (**1**) and GG-236MC (**2**).

One of the important factors in the formation of ribbonlike nanostructures and subsequent hydrogel is the molecular weight of a hydrophobic 2,3,6-tri-*O*-methyl-glucopyranosyl block. From our earlier publications, more than ten 2,3,6-tri-*O*-methyl-glucopyranosyl units are necessary to form a hydrogel.[21] The diblock copolymer having a shorter hydrophobic 2,3,6-tri-*O*-methyl-glucopyranosyl block such as G-236MC (**1**, DP_n = 10.7 and DS = 2.65) would form disk or spherical micelles rather than a ribbonlike structure. For example, the diblock co-oligomer consisting of a fully methylated cello-tetrasaccharide and unmodified cello-oligosaccharide forms self-assembled ellipsoidal particles.[38] In this study, cryo-TEM micrographs of G-236MC (**1**, DP_n = 10.7 and DS = 2.65) having fewer than ten 2,3,6-tri-*O*-methyl-glucopyranosyl units proved that the molecular weight of a hydrophobic block influenced the morphology of the self-assembled structure (disk micelle, multilamellar structure, and ribbonlike structure). Consequently, in the case of G-236MC (**1**), the number of ribbonlike supramolecular nanostructures decreased at 70 °C because of the production of disklike and multilamellar nanostructures. As a result, a hydrogel did not form. In contrast, GG-236MC (**2**, DP_n = 28.2, and DS = 2.75) having more than ten 2,3,6-tri-*O*-methyl-glucopyranosyl units formed ribbonlike supramolecular nanostructures, the number of which increased with increasing temperature, resulting in the formation of a hydrogel by the entanglement of fibrous structures and the entrapment of water molecules in their network. In the case of cryo-TEM of commercial MC (Supporting Information), sharply defined micrographs were not obtained, compared to the diblock copolymers. In addition, as far as we know, there have been no reports on the detailed structure of the fibrous structure of commercial MC. The well-defined structure of diblock copolymers **1** and **2** would be a reason that their clear micrographs compared with that of commercial MC with a complicated structure could be obtained.

CONCLUSIONS

The mechanism of hydrogel formation of real diblock MC having more than ten 2,3,6-tri-*O*-methyl-glucopyranosyl residues such as GG-236MC (**2**, DP_n = 28.2 and DS = 2.75) was investigated, and the importance of ribbonlike nanostructures consisting of GG-236MC for the supramolecular hydrogel formation was proven by means of some analytical methods tested. The cryo-TEM technique unraveled for the first time that the ribbonlike nanostructures were fabricated by self-assembly of the cellulosic diblock copolymer consisting of only saccharide chains in both hydrophilic and hydrophobic blocks. The GG-236MC is a new class of middle-molecular-weight hydrogelator. These hydrogels had a relatively tough mechanical strength compared to that of a polymer hydrogel of MC. The cryo-TEM technique also allowed us to observe the detailed morphological nanostructures formed in an aqueous solution of G-236MC (**1**, DP_n = 10.7 and DS = 2.65) and a dispersion of GG-236MC (**2**, DP_n = 28.2 and DS = 2.75) in water. Cryo-TEM observations clearly revealed that ribbonlike supramolecular nanostructures and multilamellar nanostructures were formed in water from diblock MC derivatives depending on the temperature. We found from those results that a supramolecular hydrogel forms only when many ribbonlike supramolecular nanostructures exist. At lower temperature such as 5 °C, aqueous solution does not gelate because of the absence of ribbonlike nanostructures. Furthermore, when the number of multilamellar and disklike nanostructures increased instead of increasing the number of ribbonlike nanostructures, a hydrogel also did not form in the case of G-236MC (**1**, DP_n = 10.7 and DS = 2.65). We also demonstrated that fibrous structures such as the ribbonlike nanostructures of GG-236MC (**2**, DP_n = 28.2, and DS = 2.75) indeed formed via the hydrophobic interaction between 2,3,6-tri-*O*-methyl-glucopyranosyl blocks by means of WAXS, which was also the underlying interaction and structure for the formation of a hydrogel, the same as for industrially produced MC. These key findings are attributable to the synthesis and characterization of well-defined diblock methylcelluloses with

dx.doi.org/10.1021/la3026528 | *Langmuir* 2012, 28, 12609–12618

regioselective functionalization patterns to elucidate the chemical structure of cross-linking points in industrially produced MC hydrogels.[20,21] In the future, a novel synthesis method for diblock MC analogues with DS 2.23 based on click chemistry in our recent paper[39] will permit us to synthesize diblock MC analogues with DS ≈ 1.8 and to understand the gelation mechanism of diblock MC with almost the same DS (~1.8) as that of commercial MC.

■ ASSOCIATED CONTENT

Ⓢ Supporting Information

A tilt series of cryo-TEM micrographs. A cryo-TEM micrograph of commercial MC. This material is available free of charge via the Internet at http://pubs.acs.org.

■ AUTHOR INFORMATION

Corresponding Author

*(T.H.) Tel: +49 3641 948 270. Fax: +49 3641 948 272. E-mail: thomas.heinze@uni-jena.de. (H.K.) Tel: +81-75-753-6255. Fax: +81-75-753-6300. E-mail: hkamitan@kais.kyoto-u.ac.jp.

Notes

The authors declare no competing financial interest.

■ ACKNOWLEDGMENTS

We acknowledge Professors F. Nakatsubo and T. Takano for conducting their research. EKO Instruments Co., Ltd. Osaka, Japan is gratefully acknowledged for rheological measurements. We thank Bruker AXS K.K., Yokohama, Japan for SAXS measurements. This investigation was supported in part by a Grant-in-Aid for Scientific Research from the Ministry of Education, Science, and Culture of Japan (nos. 21580205 and 24380092) and by the Japan-Germany bilateral research program from the Japanese Society for the Promotion of Sciences (JSPS) and the German Science Foundation (DFG, grant no. 446 JAP 113/341/0-1).

■ REFERENCES

(1) Lam, Y. C.; Joshi, S. C.; Tan, B. K. Thermodynamic characteristics of gelation for methyl-cellulose hydrogels. *J. Therm. Anal. Calorim.* **2007**, *87*, 475–482.

(2) Joshi, S. C.; Lam, Y. C.; Bin, C. Modelling leading to water entrapment point in thermally driven hydrogelation of methyl cellulose. *e-Polym.* **2008**, art. no. 101.

(3) Li, L. Thermal gelation of methylcellulose in water: Scaling and thermoreversibility. *Macromolecules* **2002**, *35*, 5990–5998.

(4) Nolan, C. M.; Serpe, M. J.; Lyon, L. A. Thermally modulated insulin release from microgel thin films. *Biomacromolecules* **2004**, *5*, 1940–1946.

(5) Siegel, R. A.; Firestone, B. A. pH-dependent equilibrium swelling properties of hydrophobic polyelectrolyte copolymer gels. *Macromolecules* **1988**, *21*, 3254–3259.

(6) Xu, Y.; Wang, C.; Tam, K. C.; Li, L. Salt-assisted and salt-suppressed sol-gel transitions of methylcellulose in water. *Langmuir* **2004**, *20*, 646–652.

(7) Heymann, E. Studies on sol-gel transformations. I. The inverse sol-gel transformation of methylcellulose in water. *Trans. Faraday Soc.* **1935**, *31*, 846.

(8) Kato, T.; Yokoyama, M.; Takahashi, A. Melting temperatures of thermally reversible gels. IV. Methyl cellulose-water gels. *Colloid Polym. Sci.* **1978**, *256*, 15–21.

(9) Hirrien, M.; Chevillard, C.; Desbrières, J.; Axelos, M. A. V.; Rinaudo, M. Thermogelation of methylcelluloses: new evidence for understanding the gelation mechanism. *Polymer* **1998**, *39*, 6251–6259.

(10) Joshi, S. C.; Liang, C. M.; Lam, Y. C. Effect of solvent state and isothermal conditions on gelation of methylcellulose hydrogels. *J. Biomater. Sci., Polym. Ed.* **2008**, *19*, 1611–1623.

(11) Funami, T.; Kataoka, Y.; Hiroe, M.; Asai, I.; Takahashi, R.; Nishinari, K. Thermal aggregation of methylcellulose with different molecular weights. *Food Hydrocolloids* **2007**, *21*, 46–58.

(12) Zhou, J.; Xu, Y.; Wang, X.; Qin, Y.; Zhang, L. Microstructure and aggregation behavior of methylcelluloses prepared in NaOH/urea aqueous solutions. *Carbohydr. Polym.* **2008**, *74*, 901–906.

(13) Denham, W. S.; Woodhouse, H. CLXXXVI. - The methylation of cellulose. *J. Chem. Soc., Trans.* **1913**, *103*, 1735–1742.

(14) Traube, W. Production of cellulose derivatives. *U.S. Patent 140,568* (C. A. 332,709), 1939.

(15) Burns, M. E.; Pracht, H. J. Cellulose Ethers Having a Low Molecular Weight and a High Degree of Methyl Substitution. U.S. Patent 4,048,433, 1977.

(16) Pracht, H. J.; Burns, M. E. Fabric Conditioning Compositions Containing Methylcellulose Ether. U.S. Patent .4,136,038, 1979

(17) Joshi, S. C.; Lam, Y. C. Modeling heat and degree of gelation for methyl cellulose hydrogels with NaCl additives. *J. Appl. Polym. Sci.* **2006**, *101*, 1620–1629.

(18) Ikeda, M.; Shimizu, Y.; Matsumoto, S.; Komatsu, H.; Tamaru, S. I.; Takigawa, T.; Hamachi, I. Mechanical reinforcement of a supramolecular hydrogel comprising an artificial glyco-lipid through supramolecular copolymerization. *Macromol. Biosci.* **2008**, *8*, 1019–1025.

(19) Bodvik, R.; Dedinaite, A.; Karlson, L.; Bergström, M.; Bäverbäck, P.; Pedersen, J. S.; Edwards, K.; Karlsson, G.; Varga, I.; Claesson, P. M. Aggregation and network formation of aqueous methylcellulose and hydroxypropylmethylcellulose solutions. *Colloids Surf., A* **2010**, *354*, 162–171.

(20) Nakagawa, A.; Fenn, D.; Koschella, A.; Heinze, T.; Kamitakahara, H. Synthesis of diblock methylcellulose derivatives with regioselective functionalization patterns. *J. Polym. Sci., Part A: Polym. Chem.* **2011**, *49*, 4964–4976.

(21) Nakagawa, A.; Fenn, D.; Koschella, A.; Heinze, T.; Kamitakahara, H. Physical properties of diblock methylcellulose derivatives with regioselective functionalization patterns: First direct evidence that a sequence of 2,3,6-tri-*O*-methyl-glucopyranosyl units causes thermoreversible gelation of methylcellulose. *J. Polym. Sci., Part B: Polym. Phys.* **2011**, *49*, 1539–1546.

(22) Kiyonaka, S.; Shinkai, S.; Hamachi, I. Combinatorial library of low molecular-weight organo- and hydrogelators based on glycosylated amino acid derivatives by solid-phase synthesis. *Chem.—Eur. J.* **2003**, *9*, 976–983.

(23) John, G.; Masuda, M.; Okada, Y.; Yase, K.; Shimizu, T. Nanotube formation from renewable resources via coiled nanofibers. *Adv. Mater.* **2001**, *13*, 715–718.

(24) Shimizu, T. Molecular self-assembly into one-dimensional nanotube architectures and exploitation of their functions. *Bull. Chem. Soc. Jpn.* **2008**, *81*, 1554–1566.

(25) Köhler, K.; Meister, A.; Förster, G.; Dobner, B.; Drescher, S.; Ziethe, F.; Richter, W.; Steiniger, F.; Drechsler, M.; Hause, G.; Blume, A. Conformational and thermal behavior of a pH-sensitive bolaform hydrogelator. *Soft Matter* **2006**, *2*, 77–86.

(26) Zhao, X.; Pan, F.; Xu, H.; Yaseen, M.; Shan, H.; Hauser, C. A.; Zhang, S.; Lu, J. R. Molecular self-assembly and applications of designer peptide amphiphiles. *Chem. Soc. Rev.* **2010**, *39*, 3480–98.

(27) Missirlis, D.; Chworos, A.; Fu, C. J.; Khant, H. A.; Krogstad, D. V.; Tirrell, M. Effect of the peptide secondary structure on the peptide amphiphile supramolecular structure and interactions. *Langmuir* **2011**, *27*, 6163–70.

(28) Kiyonaka, S.; Sugiyasu, K.; Shinkai, S.; Hamachi, I. First thermally responsive supramolecular polymer based on glycosylated amino acid. *J. Am. Chem. Soc.* **2002**, *124*, 10954–10955.

(29) Haque, A.; Morris, E. R. Thermogelation of methylcellulose. Part I: molecular structures and processes. *Carbohydr. Polym.* **1993**, *22*, 161–173.

(30) Li, L.; Wang, Q.; Xu, Y. Thermoreversible association and gelation of methylcellulose in aqueous solutions. *Nihon Reoroji Gakkaishi* **2003**, *31*, 287−296.
(31) Wang, Q.; Li, L. Effects of molecular weight on thermoreversible gelation and gel elasticity of methylcellulose in aqueous solution. *Carbohydr. Polym.* **2005**, *62*, 232−238.
(32) Zugenmaier, P.; Kuppel, A. Diffraction studies on trimethylcellulose and trimethylmannan. *Colloid Polym. Sci.* **1986**, *264*, 231−235.
(33) Nishida, R.; Takahashi, M. Self-assembled orientation of polymer chains in methylcellulose gel during drying process. *Polym. J.* **2007**, *40*, 148−153.
(34) Sarkar, N.; Walker, L. C. Hydration—dehydration properties of methylcellulose and hydroxypropylmethylcellulose. *Carbohydr. Polym.* **1995**, *27*, 177−185.
(35) Nishinari, K.; Hofmann, K. E.; Moritaka, H.; Kohyama, K.; Nishinari, N. Gel-sol transition of methylcellulose. *Macromol. Chem. Phys.* **1997**, *198*, 1217−1226.
(36) Desbrieres, J.; Hirrien, M.; Rinaudo, M. A calorimetric study of methylcellulose gelation. *Carbohydr. Polym.* **1998**, *37*, 145−152.
(37) Joshi, S. C.; Su, J. C.; Liang, C. M.; Lam, Y. C. Gelation of methylcellulose hydrogels under isothermal conditions. *J. Appl. Polym. Sci.* **2008**, *107*, 2101−2108.
(38) Kamitakahara, H.; Yoshinaga, A.; Aono, H.; Nakatsubo, F.; Klemm, D.; Burchard, W. New approach to unravel the structure−property relationship of methylcellulose. *Cellulose* **2008**, *15*, 797−801.
(39) Nakagawa, A.; Kamitakahara, H.; Takano, T. Synthesis and thermoreversible gelation of diblock methylcellulose analogues via Huisgen 1,3-dipolar cycloaddition. *Cellulose* **2012**, *19*, 1315−1326.

Cellulose (2012) 19:2105–2114
DOI 10.1007/s10570-012-9772-7

ORIGINAL PAPER

Synthesis of (zinc(II) phthalocyanine)-containing cellulose derivative using phthalocyanine-ring formation reaction

Yasuko Saito · Toshiyuki Takano · Keita Sakakibara · Hiroshi Kamitakahara · Fumiaki Nakatsubo

Received: 8 March 2012 / Accepted: 25 August 2012 / Published online: 6 September 2012

Abstract 2,3-Di-*O*-myristyl-6-*O*-(zinc(II) phthalocyaninyl) cellulose (**5**) was synthesized from cellulose (**1**) by five reaction steps via 6-*O*-(3′,4′-dicyanophenyl)-2,3-di-*O*-myristyl cellulose (**4**). The key reaction was phthalocyanine-ring formation on a cellulose backbone, that is, the reaction of compound **4** with *o*-phthalodinitrile in the presence of hexamethyldisilazane and zinc acetate in DMF afforded to compound **5** in 35.4 % yield. Consequently, the degree of substitution with phthalocyanine moieties of compound **5** was 0.38. The LB monolayer film of compound **5** on an indium tin oxide (ITO) electrode was found to show photocurrent generation performance at 680 nm.

Keywords Cellulose · Phthalocyanine · Phthalocyaninato zinc(II) · Regioselective · Langmuir–Blodgett film · Photocurrent generation system

Y. Saito (✉) · T. Takano · K. Sakakibara · H. Kamitakahara · F. Nakatsubo
Division of Forest and Biomaterials Science, Graduate School of Agriculture, Kyoto University, Kitashirakawa-Oiwake-cho, Sakyo-ku, Kyoto 606-8502, Japan
e-mail: ysaito@kais.kyoto-u.ac.jp

K. Sakakibara
Institute of Chemical Research, Kyoto University, Gokasho, Uji, Kyoto 611-0011, Japan

F. Nakatsubo
Research Institute for Sustainable Humanosphere, Kyoto University, Gokasho, Uji, Kyoto 611-0011, Japan

Introduction

Cellulose is the most abundant and important renewable biopolymer in nature. Recently, much attention has been paid to new applications of cellulose derivatives as advanced materials such as shape memory-recovery material (Aoki et al. 2007), material for memory device (Karakawa et al. 2007) and photoactive materials (Wondraczek et al. 2011). One of the proposed applications is the photocurrent generation system using porphyrin-containing cellulose derivatives (Sakakibara et al. 2007; Sakakibara and Nakatsubo 2008, 2010). Sakakibara and Nakatsubo (2010) have reported the fabrication of Langmuir–Blodgett (LB) films using 6-*O*-porphyrin-2,3-di-*O*-stearoyl cellulose or 6-*O*-porphyrin-2,3-di-*O*-myristoyl cellulose with high photocurrent generation performance. The cellulose backbone played an important role in the inhibition the porphyrin self-aggregation as a scaffold of porphyrin in the LB films. The effective utilization of solar light by the LB films was, however, insufficient, because the main absorption band of porphyrin (Soret band) ranges from 400 to 450 nm (Sakakibara et al. 2007). The target wavelength range for a solar cell should be considered from 400 to 920 nm (Nazeeruddin et al. 2001). To expand the range of wavelength at

which light is absorbed by the LB films, a new photosensitive dye-bearing cellulose derivative is required for the combination of the above porphyrin-containing cellulose derivatives in the films. One of the candidates for the derivative is a phthalocyanine-containing cellulose derivative, because the main adsorption band of phthalocyanine (Q bands) ranges from 600 to 700 nm (Mack and Stillman 1995). There are several reports concerning phthalocyanine-containing celluloses. For example, cotton covalently linked copper phthalocyanine trisulphonate, which is named "blue cotton" (Hayatsu 1992), cotton reacted with copper phthalocyanine (Okada et al. 1998) and cellulose nanofiber modified with cobalt tetraaminophthalocyanine (Chen et al. 2011) have been reported. However, they were surface modified celluloses with phthalocyanines, and could not be directly applied to the LB films for the photocurrent generation system. Then, 2,3-di-*O*-myristyl-6-*O*-(zinc(II) phthalocyaninyl) cellulose (**5**) was selected as a target material in our study. In target material **5**, the myristyl group (C14 alkyl group) was chosen as the *O*-2 and *O*-3 substituent groups by the following four reasons. (1) It was found in preliminary experiments, which will be published elsewhere, that the acyl groups more than fourteen carbons long were essential to good solubility in common organic solvents and formability of LB films in 6-*O*-porphyrin-2,3-di-*O*-acyl cellulose derivatives with various acyl groups from acetyl group (C2) to stearoyl group (C18). (2) The photocurrent performance of 6-*O*-porphyrin-2,3-di-*O*-myristoyl cellulose (C14 chain) has been found to be higher than that of 6-*O*-porphyrin-2,3-di-*O*-stearoyl cellulose (C18 chain) (Sakakibara and Nakatsubo 2010). (3) The alkyl group which is fourteen carbons long (C14 chain) was thought to be preferable in the combination of 6-*O*-porphyrin-2,3-di-*O*-myristoyl cellulose with C14 acyl groups to prepare a new LB film. (4) The substituent groups at *O*-2 and *O*-3 positions should be stable under alkali conditions in the synthetic route described below (Scheme 1).

There are two general methods to prepare target material **5**. One is direct introduction of *mono*-substituted phthalocyanine derivative to a cellulose backbone, and another is phthalocyanine-ring formation on a cellulose backbone using a precursor-bound cellulose derivative. In the former method, preparation of a *mono*-substituted phthalocyanine derivative is known to be time-consuming (Erdem et al. 2008), and the poor solubility of phthalocyanine derivative in common organic solvents (Allcock and Neenan 1986) may be inconvenient to homogeneous reaction for high yield synthesis of compound **5**. In the latter method, these problems may be avoided. Then, this paper describes the preparation of 2,3-di-*O*-myristyl-6-*O*-(zinc(II) phthalocyaninyl) cellulose (**5**) using the latter method, the preparation of LB monolayer films of compound **5** and preliminary evaluation of photocurrent generation performance of the LB films.

Experimental

Materials

6-*O*-(4-Methoxytrityl) cellulose (**2**) was prepared from cellulose (**1**) [Microcrystalline cellulose (Avicel®, DP_n = 141, Merck (Darmstadt, Germany))] by the conventional method (Camacho Gómez et al. 1996). The degree of substitution of 4-methoxytrityl group ($DS_{4\text{-meO-Tr}}$) and the degree of polymerization (DP_n) of compound **2** was 1.00 (determined by elementary analysis) and 138 (M_w/M_n = 3.29), respectively. [2(3),

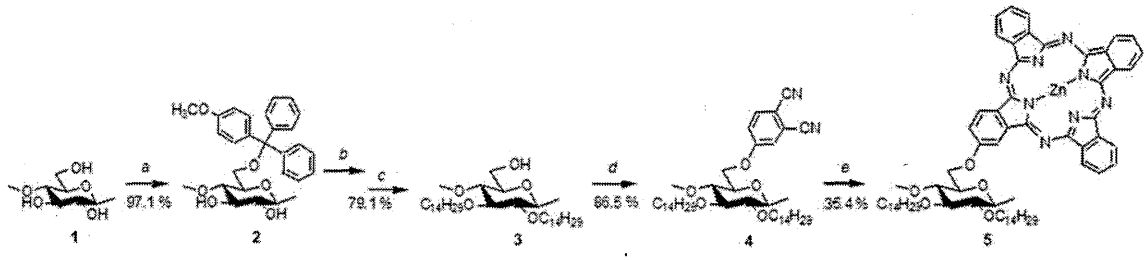

a: *p*-MeO-TrCl/Pyridine/DMAc-LiCl, 70 °C, 4h. *b*: $C_{14}H_{29}Br$/NaOH/DMSO, 70 °C, 20h. *c*: *p*-TsOH/$CHCl_3$/r.t. 12 h → r.t. 1.6 h. *d*: NO_2-$C_6H_3(CN)_2$/K_2CO_3/DMF-THF (1:4, v/v), 60 °C, 48 h. *e*: $C_6H_4(CN)_4$/$Zn(OAc)_2$/HMDS/DMF, 100 °C, 24 h.

Scheme 1 Synthetic route for 2,3-di-*O*-myristyl-6-*O*-(zinc(II) phthalocyaninyl) cellulose (**5**)

9(10),16(17),23(24)-Tetrakis(*tert*-butyl)phthalocyaninato]zinc(II) (Zn*t*BPc) was prepared according to the method of Mori et al. (2010) as a reference sample in UV–vis measurements. Zinc(II) phthalocyanine (ZnPc) was purchased from Tokyo Chemical Industry (Tokyo, Japan) as a reference sample in FTIR measurements. All other chemicals were purchased from commercial sources and used without further purification, unless otherwise specified. Tetrahydrofuran (THF) was distilled from potassium, and K_2CO_3 was dried in vacuo at 105 °C overnight before use.

2,3-Di-*O*-myristyl cellulose (**3**)

6-*O*-(4-Methoxytrityl) cellulose (**2**) (0.500 g, 1.15 mmol) was dissolved in DMSO (13 ml). 1-Bromotetradecane (1.9 ml, 6.99 mmol) was added to the solution. After the suspension was stirred at room temperature (r.t.) for 2 h, powdered NaOH (1.38 g, 34.5 mmol) and DMSO (10 ml) were added to the suspension. The reaction mixture was stirred at r.t. for 1 h and at 70 °C for 20 h. Distilled water (40 ml) was added at r.t. to dissolve the residual NaOH, and 35 % HCl (1.1 ml) was added for neutralization. The reaction mixture was extracted with $CHCl_3$. The organic layer was washed with distilled water, a saturated $NaHCO_3$ aqueous solution, distilled water, dried with Na_2SO_4, and concentrated to give an oil. The oil was added dropwise to MeOH (250 ml). The resulting precipitates were collected by centrifugation (7,300×*g*, 10 min), and dried in vacuo at 70 °C to give crude products (0.956 g).

To the solution of the products in $CHCl_3$ (10 ml), *p*-toluenesulfonic acid monohydrate (*p*-TsOH) (0.438 g, 2.30 mmol) was added. The reaction solution was stirred at r.t. for 12 h, and added dropwise to EtOH (175 ml). The resulting precipitates were collected by centrifugation (14,000×*g*, 10 min), dried in vacuo at r.t., and dissolved in $CHCl_3$ (6 ml). After addition of *p*-TsOH (0.218 g, 1.15 mmol) to the solution, the reaction mixture was kept at r.t. for 1.6 h, and added dropwise to EtOH (150 ml). The resulting precipitates were collected by centrifugation (410×*g*, 10 min), and dissolved in a small amount of $CHCl_3$. The solution was added dropwise in acetone (150 ml). The resulting precipitates were collected by centrifugation (14,000×*g*, 10 min), washed with acetone and EtOH, and dried in vacuo at 65 °C overnight to afford compound **3** (0.444 g, 79.1 % yield).

Compound **3**; $DS_{myristyl}$: 1.66 (determined by elementary analysis); DP_n: 38 (M_w/M_n = 1.69); ^1H NMR ($CDCl_3$): δ 4.31 (H-1), 3.93 (H-6a), 3.88-3.42 (H-6b, myristyl –O–CH_2–, H-4), 3.26 (H-3, H-5), 2.96 (H-2), 1.52 (myristyl –OCH_2–CH_2–), 1.14–1.31 (myristyl –CH_2–), 0.83–0.91 (myristyl –CH_3) ppm; ^{13}C NMR ($CDCl_3$), δ 102.9 (C-1), 83.0 (C-3), 82.2 (C-2), 78.1 (C-4), 75.1 (C-5), 73.9, 73.5 (myristyl –OCH_2–), 61.6 (C-6), 31.9, 30.4, 30.3, 29.7, 29.6, 29.3, 26.2, 22.6 (myristyl –CH_2–), 14.1 (myristyl –CH_3) ppm; FTIR (KBr): ν 3423, 2926, 2854, 1463, 1369, 1103, 1068 cm^{-1}.

6-*O*-(3′,4′-Dicyanophenyl)-2,3-di-*O*-myristyl cellulose (**4**)

To the solution of 2,3-di-*O*-myristyl cellulose (**3**) (0.350 g, 0.718 mmol) in DMF/THF (1/4, v/v) (35 ml), 4-nitrophthalonitrile (0.546 g, 3.15 mol) and K_2CO_3 (0.872 g, 6.31 mmol) were added. The reaction mixture was stirred at 60 °C for 48 h, and was poured into EtOH (175 ml). The resulting precipitates were collected by centrifugation (14,000×*g*, 12 min), and washed with EtOH, EtOH/H_2O (1/1, v/v), and EtOH to give crude products. The products were purified by the re-precipitation method from EtOH again to give compound **4** (0.363 g, 86.5 % yield).

Compound **4**; $DS_{dicyanophenyl}$: 0.76 (determined by elementary analysis); DP_n: 20 (M_w/M_n = 1.28); ^1H NMR ($CDCl_3$): δ 7.90–7.59 (H-5′), 7.32–7.08 (H-2′, H-6′), 4.80–2.83 (cellulose ring-H, myristyl –OCH_2–), 1.60–1.39 (myristyl –OCH_2–CH_2–), 1.35–1.02 (myristyl –CH_2–), 0.89–0.86 (myristyl –CH_3) ppm; ^{13}C NMR ($CDCl_3$): δ 161.5 (C-1′), 135.1 (C-5′), 119.7 (C-2′, C-6′), 117.5 (C-3′), 115.5 (C4′-*C*N), 115.0 (C3′-*C*N), 108.0 (C-4′), 103.1 (C-1), 83.0 (C-3), 81.9 (C-2), 78.1 (C-4), 75.2 (C-5), 73.6 (myristyl –OCH_2–), 67.1(C-6 substituted), 61.5 (C-6 unsubstituted), 31.9, 30.4, 30.3, 29.7, 29.6, 29.3, 26.2, 22.6 (myristyl –CH_2–), 14.1 (myristyl –CH_3) ppm; FTIR (KBr): ν 3442, 2926, 2854, 2233 (CN), 1600, 1097, 1066 cm^{-1}; UV–vis (in $CHCl_3$): λ (log ε) 305 (3.5), 296 (3.5), 258 (4.1) nm.

2,3-Di-*O*-myristyl-6-*O*-(zinc(II) phthalocyaninyl) cellulose (**5**)

6-*O*-(3′,4′-Dicyanophenyl)-2,3-di-*O*-myristyl cellulose (**4**) (0.100 g, 0.172 mmol) was suspended in DMF (3.0 ml). After stirring at 100 °C for 3.3 h, 1,1,1,3,3,3-hexamethyldisilazane (HMDS) (1.3 ml,

6.23 mmol) was added. The reaction mixture was stirred at r.t. for 2.2 h and at 100 °C for 30 min. Zinc acetate (141 mg, 0.770 mmol), *o*-phthalodinitrile (376 mg, 2.94 mmol) and HMDS (0.7 ml, 3.35 mmol) were added to the mixture. The mixture was stirred under nitrogen atmosphere at 100 °C for 24 h, and was poured into MeOH (200 ml). The resulting blue precipitates were collected by centrifugation (14,000×*g*, 10 min), and suspended in $CHCl_3$ (30 ml). The suspension was stirred at r.t. overnight, and filtered with $CHCl_3$ to remove by-products such as zinc(II) phthalocyanine. The filtrate was concentrated to give crude products. The products were purified by the re-precipitation method from MeOH (150 ml) to afford the purified product. The product was further dissolved in a small amount of $CHCl_3$ and filtered with a syringe filter (0.45 μm, Minisart RC 15) to remove the insoluble fraction, and concentrated to afford compound **5** (0.0485 g, 35.4 % yield). (The yield was calculated based on the assumption that the residual dicyanophenyl groups did not react with phthalodinitrile and that the residual hydroxyl groups were trimethylsilylated as described below.)

Compound **5**; $DS_{phthalocyanine}$: 0.38 (determined by UV–vis method); DP_n: 25 (M_w/M_n = 2.20); ^1H NMR ($CDCl_3$): δ 9.82–7.05 (zinc(II) phthalocyaninyl-H, dicyanophenyl-H), 4.80–2.76 (cellulose ring-H, myristyl-OCH_2–), 1.96–0.49 (myristyl –CH_2–, and –CH_3), 0.07 (–$Si(CH_3)_3$) ppm; FTIR (KBr): ν 2924, 2852, 2231 (CN), 1487, 1332, 1111, 1091, 1060, 723 cm^{-1}; UV–vis (in $CHCl_3$): λ (log ε) 676 (4.3), 617 (3.8), 339 (4.1), 243 (4.2) nm.

Preparation of Langmuir–Blodgett films of compound 5

A diluted solution of compound **5** in $CHCl_3$ (0.5 mg ml^{-1}) was spread onto a water subphase in a Teflon-coated trough (331 × 100 × 5 mm, USI-3-22T, USI). The ultrapure water purified by Mili-Q (Nihon Millipore) was used for the subphase. The solvent was evaporated for 30 min. The surface pressure (π)-area (A) isotherm was measured at a constant compression rate of 6 mm min^{-1}. The surface pressure was measured using a film balance of Wilhelmy type. The vertical dipping method was used to deposit the surface monolayer onto a substrate. The upward and downward stroke rate was 6 mm min^{-1}. During the deposition, the surface pressure was controlled to remain 10 mN m^{-1} and the surface temperature was kept at 20 °C to prepare the LB films.

Measurements

FTIR spectra were recorded in KBr pellets with a Shimadzu IRPrestige-21 spectrophotometer. ^1H and ^{13}C NMR spectra were recorded on a Varian 500 MHz NMR spectrometer in $CDCl_3$ with TMS as an internal standard. Chemical shift (δ) was given in δ values (parts per million). UV–vis spectra were recorded on a Jasco V-560 UV–vis spectrophotometer in $CHCl_3$. Gel permeation chromatography (GPC) was performed using a Shimadzu LC-10 system equipped with a Shimadzu UV–vis detector (SPD-10Avp) and a Shimadzu RI detector (RID-10A) (Conditions: columns: Shodex columns K-802, K-802.5 and K-805 (connected in series); column temperature: 40 °C; eluent: $CHCl_3$; flow rate : 1.0 ml min^{-1}; standards: polystyrene standards (Shodex)). Wavelength of UV detection was 600 nm for compounds **4** and **5**, or 254 nm for other compounds. AFM observation of the monolayer film was performed in dynamic mode using a Shimadzu SPM-9600 equipped with a tetrahedral shaped silicon cantilever (AC240TS-C2, Olympus). The photocurrent measurements were performed according to the method reported by Sakakibara and Nakatsubo (2010).

Results and discussion

Preparation of 2,3-di-*O*-myristyl-6-*O*-(zinc(II) phthalocyaninyl) cellulose (5)

The synthetic route of 2,3-di-*O*-myristyl-6-*O*-(zinc(II) phthalocyaninyl) cellulose (**5**) from cellulose (**1**) is shown in Scheme 1. 6-*O*-(4-Methoxytrityl) cellulose (**2**) was prepared from cellulose (**1**) in 97.1 % yield by the conventional method (Camacho Gómez et al. 1996).

Kasai et al. (2005) has reported the preparation of 2,3-di-*O*-octadecylcellulose from 6-*O*-(4-methoxytrityl) cellulose with 1-bromooctadecane/NaOH powder/DMSO/a small amount of water at 70 °C for 20 h. Myristylation of compound **2** was performed with 1-bromotetradecane/NaOH powder/DMSO at 70 °C for 20 h, because it was found that a small amount of water was not necessary to our reaction in a

preliminary experiment. The addition order of NaOH powder and 1-bromotetradecane was important in the myristylation. When NaOH powder was added to the solution of compound **2** at first, the reaction mixture became to be too viscous for dispersion of 1-bromotetradecane. 1-Bromotetradecane should be first added to the solution in the myristylation. The purification of 6-*O*-(4-methoxytrityl) 2,3-di-*O*-myristyl cellulose was very difficult because of the similar solubility behaviors in common organic solvents of 6-*O*-(4-methoxytrityl)-2,3-di-*O*-myristyl cellulose, the residual 1-bromotetradecane, and the by-products from 1-bromoteradecane such as 1-tetradecanol. It has been also reported that the purification of 6-*O*-(4-methoxytrityl)-2,3-di-*O*-octadecyl cellulose was laborious and tedious work (Kasai et al. 2005). Indeed, the re-precipitation method was not effective for the purification of 6-*O*-(4-methoxytrityl)-2,3-di-*O*-myristyl cellulose, although several organic solvents for the re-precipitation were tried. Then, the crude myristylated products after one re-precipitation from MeOH were subjected to de(4-methoxy)tritylation, because de(4-methoxy)tritylation proceeded smoothly and the purification of 2,3-di-*O*-myristyl cellulose (**3**) was relatively easy, even in the presence of the residual 1-bromotetradecane and the resulting by-products in a preliminary experiment. De(4-methoxy)tritylation of the crude myristylation products with *p*-toluenesulfonic acid in $CHCl_3$ at r.t. for 12 h afforded the de(4-methoxy)tritylated product. However, the ^{1}H-NMR spectrum of the product showed that a small amount of (4-methoxy)trityl group remained (data not shown). De(4-methoxy)tritylation of the product was conducted at r.t. for 1.6 h again to afford compound **3** in 79.1 % yield (based on compound **2**). The bands at 1606 and 1508 cm^{-1} derived from (4-methoxy)trityl group were not present in the FTIR spectrum of compound **3** (Fig. 1b) and the signals at 7.0–8.0 ppm derived from aromatic-H were not present in the ^{1}H NMR spectrum of compound **3** (Fig. 2a), suggesting that de(4-methoxy)tritylaion completely proceeded. The completion of reaction was also supported by the ^{13}C NMR spectrum of compound **3** (Fig. 2b). The CH stretching vibrations at 2926 and 2854 cm^{-1} assigned to myristyl group were present in the FTIR spectrum of compound **3** (Fig. 1b) and the signals at 0.83–1.52 ppm derived from myristyl group-H were present in the ^{1}H NMR spectrum of compound **3** (Fig. 2a). The $DS_{myristyl}$ of compound **3** was calculated

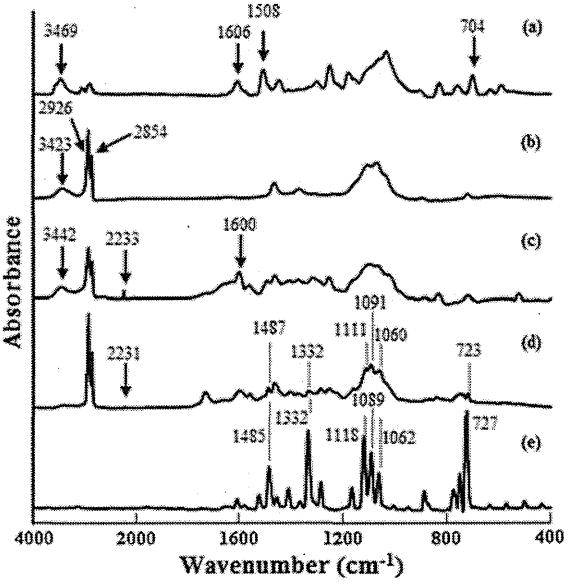

Fig. 1 FTIR spectra of compounds **2** (**a**), **3** (**b**), **4** (**c**), **5** (**d**) and ZnPc (**e**)

to be 1.66 by elementary analysis. The DP_n of compound **2** decreased from 138 to 38 during myristylation and the following de(4-methoxy)tritylation. One of the reason is the acidic hydrolysis proceeding as a side reaction in de(4-methoxy)tritylation. Compound **3** was soluble in $CHCl_3$ and THF, but insoluble in DMSO and DMF.

The treatment of alcohol with 4-nitrophthalonitrile in the presence of K_2CO_3 in DMF gave the corresponding 4-alkoxyphthalonitrile (Álvarez-Micó et al. 2007; Choi et al. 2008). Then, compound **3** was treated with the reagents in DMF at 60 °C for 24 h to give 6-*O*-(3′,4′-dicyanophenyl)-2,3-di-*O*-myristyl cellulose (**4**) in 77.0 % yield. However, the $DS_{dicyanophenyl}$ of compound **4** was 0.41, which is easily evaluated by ^{1}H NMR. The low DS seemed to be due to the heterogeneous reaction in DMF. The mixed solvents of DMF and THF with various ratios were investigated (Table 1). When DMF/THF (1/4, v/v) and THF were used, the reactions were homogeneous systems. Consequently, it was found that DMF/THF (1/4, v/v) was the best solvent to achieve a high $DS_{dycianopphenyl}$ of compound **4** (Entry 3). The characteristic band derived from the nitrile group of the dicyanophenyl group at 2233 cm^{-1} (Bilgin et al. 2008) was found in the FTIR spectrum of compound **4** (Fig. 1c). The signals at 7.90–7.59 and 7.32–7.08 ppm and the signals at 115.0 and 115.5 ppm derived from dicyanophenyl group

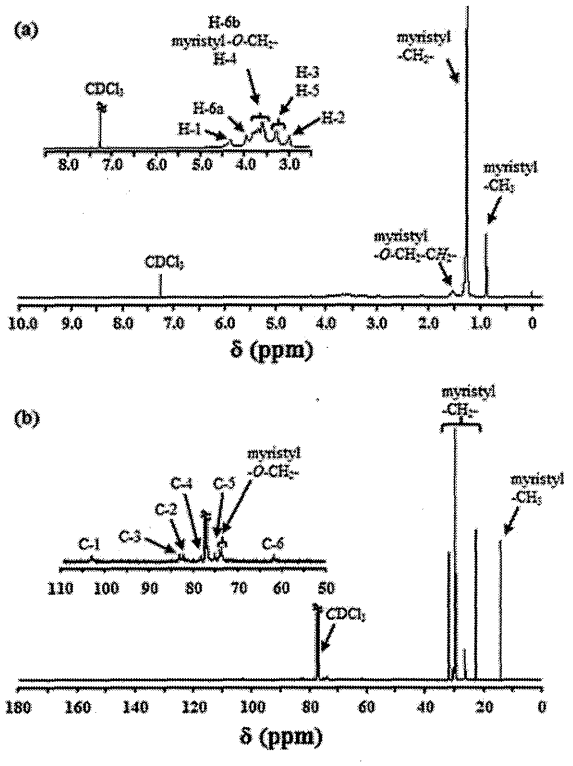

Fig. 2 NMR spectra of compound **3** (in $CDCl_3$). ^1H NMR (**a**), ^{13}C NMR (**b**)

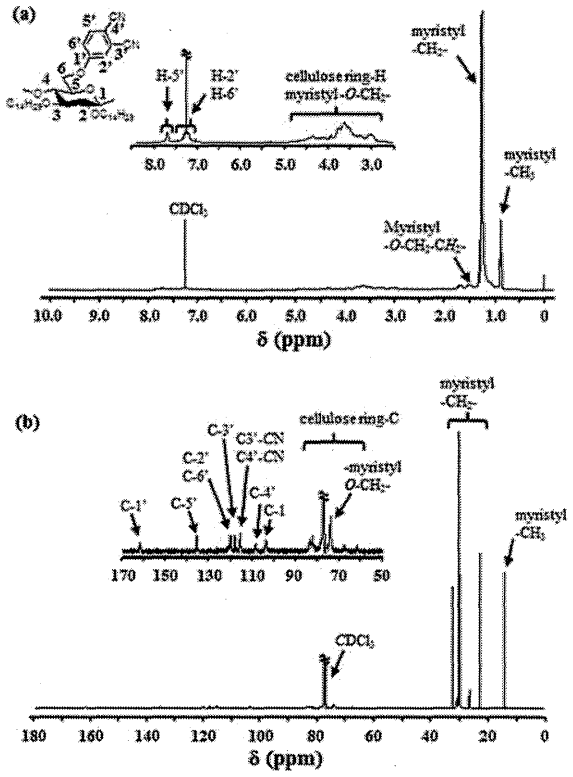

Fig. 3 NMR spectra of compound **4** (in $CDCl_3$). ^1H NMR (**a**), ^{13}C NMR (**b**)

Table 1 Results of dicyanophenylation

Entry	DMF/THF (v/v)	$DS^a_{dicyanophenyl}$	Yield
1	1/0	0.41	77
2	4/1	0.35	71
3	1/4	1.10	73
4	0/1	0.71	73

[a] Determined by ^1HNMR method

(Álvarez-Micó et al. 2007) were observed in the ^1H NMR (Fig. 3a) and ^{13}C NMR spectra, respectively. These results suggested that dicyanophenylation proceeded as expected. The $DS_{dicyanophneyl}$ of compound **4** (Entry 3) was finally determined by elementary analysis, and found to be 0.90. The DP_n of compound **3** was decreased from 38 to 20 during dicyanophenylation. It was due to alkali hydrolysis in dicynaophenylation, although further investigation was required.

There were two problems to be considered in phthalocyanine-ring formation at C-6 position of compound **4** with phthalodinitrile. One possibility was that depolymerization of the cellulose backbone might occur simultaneously with phthalocyanine-ring formation because compound **4** should be subjected to the ring-formation reaction under hard reaction conditions. For example, the ring formations on precursor-bounded polymers with phthalodinitrile derivative/CuBr/dry DMF at 165 °C for 3.5 h (Allcock and Neenan. 1986), and that with phthalodinitrile derivative/$ZnCl_2$/quinoline, at 210–230 °C for 3 h (Zhang et al. 2006) and that with phthalodinitrile derivative/[dry DMF/2-dimethylaminoethanol (1/1, v/v)] under reflux for 20 h (Leznoff and Hall 1982) have been reported. Another possibility was that two or more 3,4-dicyanophenyl groups attached to the same or different cellulose chains might be incorporated into the same phthalocyanine ring. Therefore, mild conditions (especially lower reaction temperature) and dilute conditions were required in our reaction. Uchida et al. (2002) have reported that the reaction of phthalodinitrile in the presence of $Zn(OAc)_2$ and HMDS in DMF under mild conditions (at 100 °C for 10 h) afforded zinc(II) phthalocyanine in 73 % yield. The method under dilute conditions was applied to the

phthalocyanine-ring formation at C-6 position of compound **4**. The reaction of compound **4** with phthalodinitrile in the presence of $Zn(OAc)_2$ and HMDS in DMF at 100 °C for 24 h gave 2,3-di-*O*-myristyl-6-*O*-(zinc(II) phthalocyaninyl) cellulose (**5**) as a dark blue product in 35.4 % yield.

Compound **5** was firstly subjected to FTIR, UV–vis and NMR measurements to confirm phthalocyanine-ring formation. The characteristic bands at 1487, 1332, 1111, 1091, 1060, 723 cm^{-1} derived from zinc(II) phthalocyanine (Leznoff et al. 1991; Seoudi et al. 2005) were present (Fig. 1d). Those bands were in good agreement with the bands in the FTIR spectrum of ZnPc (Fig. 1e). The band at 2231 cm^{-1} from nitrile groups was still present, although it was very small (Fig. 1d). The Q bands around 600–700 nm and the Soret band around 300–400 nm were clearly observed in the UV–vis spectrum of compound **5** as well as that of Zn*t*BPc, whereas they were not observed in that of compound **4** (Fig. 4i). These results indicated that phthalocyanine-ring was formed as expected, although some dicyanophenyl groups did not react. On the other hand, the bands around 3400 cm^{-1} were not present in

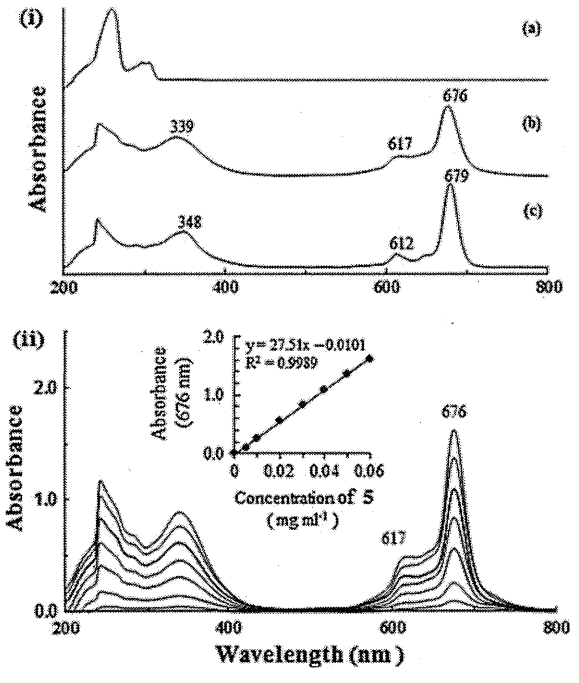

Fig. 4 **i** UV–vis spectra of compounds **4** (*a*), **5** (*b*) and Zn*t*BPc (*c*). **ii** UV–vis spectra of compound **4** in $CHCl_3$ at different concentrations: 0.06, 0.05, 0.04, 0.03, 0.02, 0.01, 0.005 mg ml^{-1} from the top. The inset shows plot of the absorbance at 676 nm against the concentration

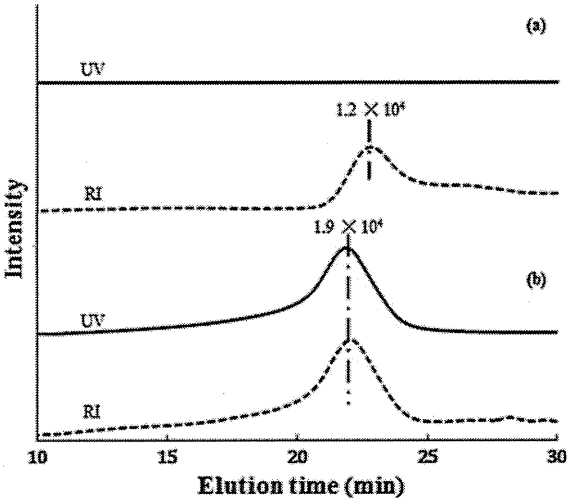

Fig. 5 GPC elution curves of compounds **4** (**a**) and **5** (**b**) (UV detection wavelength was 600 nm)

the FTIR spectrum of compound **5** (Fig. 1d). The strong peak around 0.07 ppm was observed in the spectrum of ^1H NMR of compound **5** (Fig. 6). Considering that HMDS is also known as a silylating agent (Deng 2011; Wang et al. 2006; Cooper et al. 1981), it was suggested that residual hydroxyl groups of compound **4** were trimethylsilylated during the phthalocyanine-ring formation. Next, compound **5** was subjected to Gel Permeation Chromatography (GPC) to confirm that phthalocyanine units were covalently attached to the cellulose backbone. Figure 5 shows GPC elution curves by RI and UV detectors of compounds **4** and **5**. The RI and UV elution curves of compound **5** showed nearly identical elution profiles (Fig. 5b), and the peak at low molecular weight corresponding to free zinc(II) phthalocyanine, was not present in the UV elution curve of compound **5**. These results suggested that compound **5** was phthalocyanine-bearing cellulose derivative. Next, the $DS_{phthalocyanine}$ of compound **5** was investigated. Allcock and Neenan (1986) has been reported that the spectrum of monomeric copper(II) phthalocyanine consists of strong adsorption at 670 nm and the weak adsorption at 605 nm derived from Q bands, and that of dimeric phthalocyanine consists of the two bands of almost equal intensity. Figure 4ii shows the UV–vis spectra of compound **5** in $CHCl_3$ at different concentrations in the range of 0.005–0.06 mg ml^{-1}. The strong adsorption at 676 nm was present in all UV–vis spectra. Any bands, due to aggregation (Huang et al.

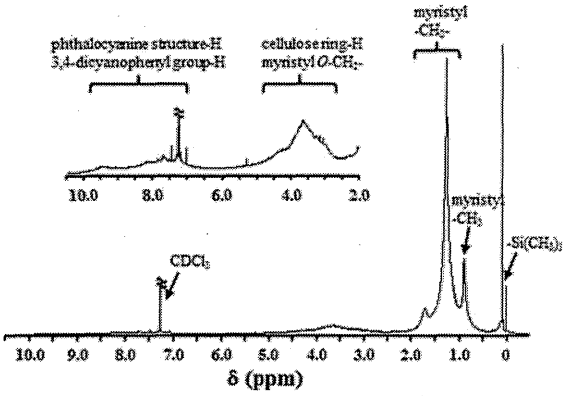

Fig. 6 ^{1}H NMR spectrum of compound **5** in $CDCl_3$

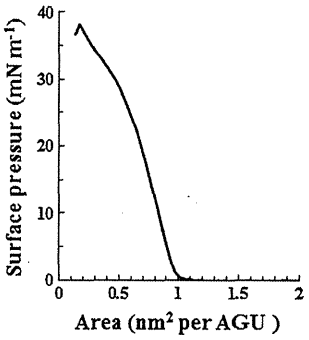

Fig. 7 Surface pressure (π)-area (A) isotherm of compound **5**

2007), were not present at the Q band, and the intensity of the Q bands increased proportionally with an increase of concentration of compound **5**. On the other hand, the Q bands were not present in UV–vis spectrum of compound **4** (Fig. 4i). Therefore, the $DS_{phthalocyanine}$ of compound **5** could be estimated by UV–vis method (UV detection: 676 nm) with calibration curves from Zn*t*BPc. Consequently, the $DS_{phthalocyanine}$ was calculated to be 0.38. Finally, the DP_n of compound **5** was calculated using the following Eq (1) on the assumption that the residual dicyanophenyl group did not react with phthalodinitrile and that the residual hydroxyl groups were completely trimethylsilylated.

$$\begin{aligned} DP_n = M_n / [&(\text{a ring–formed unit } (1082)) \times 0.38 \\ &+ (\text{a not ring–formed unit with dicyanophenyl group}(639)) \times 0.38 \\ &+ (\text{a not ring–formed unit without dicyanophenyl group } (585) \times 0.24] \end{aligned} \quad (1)$$

The DP_n of compound **5** was estimated to be 25 whereas the DP_n of compound **4** was calculated to be 20, suggesting that cross-linking reaction proceeded to some extent during the phthalocyanine-ring formation.

Preparation of LB films of compound **5** and preliminary evaluation of photocurrent generation performance

Figure 7 shows the surface pressure (π)-area (A) isotherm of compound **5** at the air–water interface at 20 °C. The limiting molecular area was 0.98 nm^2 per anhydro glucose unit, obtained by the extrapolation of the steepest part of the isotherm to zero surface pressure. The cross-sectional areas of a glucopyranose ring and a phthalocyanine core are known to be ca. 0.55–0.60 nm^2 (Sakakibara et al. 2007) and ca. 1.00 nm^2 (Cook and Chambrier 2003), respectively. The average area occupied per unsubstituted phthalocyanine core is reported to be ca. 0.40 nm^2 if the molecules lie perpendicular to the water (Cook and Chambrier 2003). It was therefore suggested that the phthalocyanine units of compound **5** were oriented almost perpendicular to the water surface.

6-*O*-Porphyrin-2,3-di-*O*-stearoyl cellulose monolayer has been reported to be successfully deposited onto several substrates at surface pressure of 10 mN m^{-1} by the horizontal lifting method (Sakakibara et al. 2007). Then, the horizontal lifting method was tried to prepare of a LB monolayer film of compound **5**. The monolayer transfers with various surface pressures on various substrates, however, were unsuccessful. The vertical dipping method was applied to the LB monolayer film preparation. The monolayer of compound **5** could be transferred onto mica at surface pressure of 10 mN m^{-1} by upward stroke but not by downward stroke. Figure 8 shows AFM image of the monolayer film of compound **5** on mica. It is shown that the surface was almost smooth and homogeneous, although some aggregates of ca. 100 nm in diameter were observed. The LB monolayer of compound **5** was also successfully transferred onto quartz and Indium tin oxide (ITO) electrode by the vertical dipping method. Figure 9 shows UV–vis spectra of the LB monolayer film of compound **5** on quartz and the solution of compound **5** in $CHCl_3$. It has been reported that the red-sift and blue-shift of the Q bands of phthalocyanine were observed in the J-aggregates and H-aggregates, respectively (Huang et al. 2007). The Q band of the monolayer film and the

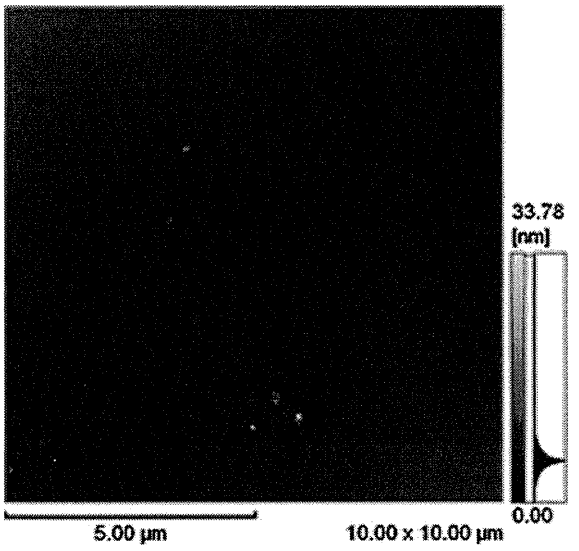

Fig. 8 AFM image of the monolayer of compound **5** deposited on freshly cleaved mica at a surface pressure of 10 mN m^{-1} at 20 °C

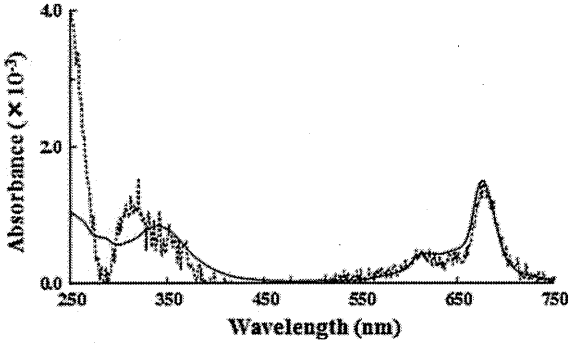

Fig. 9 UV–vis absorption spectra of the LB monolayer (*solid line*) and the solution in $CHCl_3$ (0.04 mg ml^{-1}) (*dotted line*) of compound **5** (normalized at 676 nm)

solution of compound **5** were observed at almost same position, suggesting that the cellulose scaffold effectively suppressed the aggregation of the phthalocyanine moieties.

Photocurrent measurement at 680 nm was performed for the LB monolayer film of compound **5** on an ITO electrode (transfer ratio = 1.01) as a preliminary evaluation of photocurrent generation performance. Figure 10 shows the photocurrent generation of the LB monolayer at 680 nm. A steady state anodic photocurrent of which photocurrent density was 0.45 nA cm^{-2} appeared during light illumination, although the performance was low. The preparation

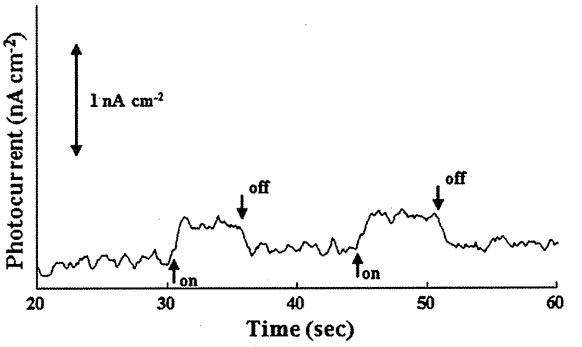

Fig. 10 Photoelectrochemical response of the monolayer of compound **5** on an ITO electrode with illumination at 680 nm

and evaluation of the mixed LB films of compound **5** and the porphyrin-containing cellulose derivatives without any aggregations are now investigating at the next step of our study.

Conclusions

2,3-Di-*O*-myristyl-6-*O*-(zinc(II) phthalocyaninyl) cellulose with the $DS_{phthalocyaninse}$ of 0.38 (**5**) was prepared from cellulose (**1**) using phthalocyanine-ring formation on the cellulose backbone by five reaction steps in 23.5 % overall yield. Compound **5** is the first regioselectively substituted phthalocyaine cellulose derivative. The LB monolayer film of compound **5** on mica, quartz and ITO substrates could be prepared by the vertical dipping method, although some aggregates were observed in AFM image of the monlayer. The LB monolayer film of compound **5** showed photocurrent performance at 680 nm, whereas the LB monolayer films of the porphyrin-containing celluloses generated photocurrent in the range of 400–600 nm (Sakakibara and Nakatsubo 2010). Compound **5** is expected to be a complementary material of the porphyrin-containing cellulose derivatives for solar cell materials.

References

Allcock HR, Neenan TX (1986) Synthesis of polyphosphazenes bearing covalently linked copper phthalocyanine units. Macromolecules 19:1495–1501. doi:10.1021/ma00160a001

Álvarez-Micó X, Calvete MJF, Hanack M, Ziegler T (2007) Expeditious synthesis of glycosylated phthalocyanines. Synthesis 14:2186–2192. doi:10.1055/s-2007-983753

Aoki D, Teramoto Y, Nishio Y (2007) SH-containing cellulose acetate derivatives: preparation and characterization as a shape memory-recovery material. Biomacromolecules 8:3749–3757. doi:10.1021/bm7006828

Bilgin A, Yağci Ç, Mendi A, Yıldız U (2008) Synthesis and characterization of new monomeric and polymeric phthalocyanines. J Appl Polym Sci 110:2115–2126. doi:10.1002/app.28774

Camacho Gómez JA, Erler UW, Klemm DO (1996) 4-Methoxy substituted trityl groups in 6-*O* protection of cellulose: homogeneous synthesis, characterization, detritylation. Macromol Chem Phys 197:953–964

Chen S-L, Huang X-J, Xu Z-K (2011) Functionalization of cellulose nanofiber mats with phthalocyanine for decoloration of reactive dye wastewater. Cellulose 18:1295–1303. doi:10.1007/s10570-011-9572-5

Choi C-F, Huang J-D, Lo P-C, Fong W-P, Ng DKP (2008) Glycosylated zinc(II) phthalocyanines as efficient photosensitizers for photodynamic therapy. Synthesis, photophysical properties and in vitro photodynamic activity. Org Biomol Chem 6:2173–2181. doi:10.1039/b802212g

Cook MJ, Chambrier I (2003) Phthalocyanine thin films: deposition and structural studies. In: Kadish KM, Smith KM, Guilard R (eds) The porphyrin handbook, vol 17. Elsevier Science, USA, pp 62–103

Cooper GK, Sandberg KR, Hinck JF (1981) Trimethylsilyl cellulose as precursor to regenerated cellulose fiber. J Appl Polym Sci 26:3827–3836. doi:10.1002/app.1981.070261129

Deng X (2011) Hexamethyldisilazane. Synlett 6:881–882. doi:10.1055/s-0030-1259911

Erdem SS, Nesterova IV, Soper SA, Hammer RP (2008) Solid-phase synthesis of asymmetrically substituted "AB_3-Type" phthalocyanines. J Org Chem 73:5003–5007. doi:10.1021/jo800536v

Hayatsu H (1992) Cellulose bearing covalently linked copper phthalocyanine trisulphonate as an adsorbent selective for polycyclic compounds and its use in studies of environmental mutagens and carcinogens. J Chromatogr 597:37–56. doi:10.1016/0021-9673(92)80095-C

Huang X, Zhao F, Li Z, Huang L, Tang Y, Zhang F, Tung C-H (2007) A novel self-aggregates of phthalocyanine based on Zn–O coordination. Chem Lett 36:108–109. doi:10.1246/cl.2007.108

Karakawa M, Chikamatsu M, Yoshida Y, Azumi R, Yase K, Nakamoto C (2007) Organic memory device based on carbazole-substituted cellulose. Macrolmol Rapid Commun 28:1479–1484. doi:10.1002/marc.200700186

Kasai W, Kuga S, Magoshi J, Kondo T (2005) Compression behavior of Langmuir–Blodgett monolayers of regioselectively substituted cellulose ethers with long alkyl side chains. Langmuir 21:2323–2329. doi:10.1021/la047323j

Leznoff CC, Hall TW (1982) The synthesis of a soluble, unsymmetrical phthalocyanine on a polymer support. Tetrahedron Lett 23:3023–3026

Leznoff CC, Svirskaya PI, Khouw B, Cerny RL, Seymour P, Lever ABP (1991) Synthesis of monometalated and unsymmetrically substituted binuclear phthalocyanines and a pentanuclear phthalocyanine by solution and polymer support methods. J Org Chem 56:82–90

Mack J, Stillman MJ (1995) Band deconvolution analysis of the absorption and magnetic circular dichroism spectral data of ZnPc(-2) recorded at cryogenic temperatures. J Phys Chem 99:7935–7945. doi:10.1021/j100020a015

Mori S, Nagata M, Nakahata Y, Yasuta K, Goto R, Kimura M, Taya M (2010) Enhancement of incident photon-to-current conversion efficiency for phthalocyanine-sensitized solar cells by 3D molecular structuralization. J Am Chem Soc 132:4054–4055. doi:10.1021/ja9109677

Nazeeruddin MK, Péchy P, Renouard T, Zakeeruddin SM, Humphry-Baker R, Comte P, Liska P, Cevery L, Costa E, Shklover V, Spiccia L, Deacon GB, Bignozzi CA, Grätzel M (2001) Engineering of efficient panchromatic sensitizers for nanocrystalline TiO_2-based solar cells. J Am Chem Soc 123:1613–1624. doi:10.1021/ja003299u

Okada Y, Fukuoka F, Morita Z (1998) Environmental effects of oxygen on the fading of monochlorotriazinyl reactive dyes on cotton fabrics. Dyes Pigm 37:47–64

Sakakibara K, Nakatsubo F (2008) Effect of fullerene on photocurrent performance of 6-*O*-porphyrin-2,3-di-*O*-stearoylcellulose Langmuir–Blodgett films. Macromol Chem Phys 209:1274–1281. doi:10.1002/macp.200800027

Sakakibara K, Nakatsubo F (2010) Effect of central metals in the porphyrin ring on photocurrent performance of cellulose Langmuir-Blodgett films. Macromol Chem Phys 211:2425–2433. doi:10.1002/macp.201000257

Sakakibara K, Ogawa Y, Nakatsubo F (2007) First cellulose Langmuir–Blodgett films towards photocurrent generation systems. Macromol Rapid Commun 28:1270–1275. doi:10.1002/marc.200700130

Seoudi R, El-Bahy GS, El Sayed ZA (2005) FTIR, TGA and DC electrical conductivity studies of phthalocyanine and its complexes. J Mol Struct 753:119–126. doi:10.1016/j.molstruc.2005.06.003

Uchida H, Tanaka H, Yoshiyama H, Reddy PY, Nakamura S, Toru T (2002) Novel synthesis of phthalocyanines from phthalonitriles under mild conditions. Synlett 10:1649–1652

Wang C, Tan H, Dong Y, Shao Z (2006) Trimethylsilyl hydroxypropyl cellulose: preparation, properties and as precursors to graft copolymerization of ε-caprolactone. React Funct Polym 66:1165–1173. doi:10.1016/j.reactfunctpolym.2006.02.006

Wondraczek H, Kotiaho A, Fardim P, Heinze T (2011) Photoactive polysaccharides. Carbohydr Polym 83:1048–1061. doi:10.1016/j.carbpol.2010.10.014

Zhang Y, Niu Y, Xu R, Wang G, Jiang Z (2006) Synthesis and characterization of poly(aryl ether sulfone)s with metallophthalocyanine pendant unit. J Appl Polym Sci 102:3457–3461. doi:10.1002/app.24498

Planta (2013) 237:705–715
DOI 10.1007/s00425-012-1784-x

ORIGINAL ARTICLE

Immunolocalization of 8-5′ and 8-8′ linked structures of lignin in cell walls of *Chamaecyparis obtusa* using monoclonal antibodies

Shingo Kiyoto · Arata Yoshinaga · Naoyuki Tanaka · Munehisa Wada · Hiroshi Kamitakahara · Keiji Takabe

Received: 15 June 2012 / Accepted: 11 October 2012 / Published online: 30 October 2012

Abstract Mouse monoclonal antibodies were generated against dehydrodiconiferyl alcohol- or pinoresinol-*p*-aminohippuric acid (*p*AHA)-bovine serum albumin (BSA) conjugate as probes that specifically react with 8-5′ or 8-8′ linked structure of lignin in plant cell walls. Hybridoma clones were selected that produced antibodies that positively reacted with dehydrodiconiferyl alcohol- or pinoresinol-*p*AHA–BSA and negatively reacted with *p*AHA–BSA and guaiacylglycerol-beta-guaiacyl ether-*p*AHA–BSA conjugates containing 8-*O*-4′ linkage. Eight clones were established for each antigen and one of each clone that positively reacted with wood sections was selected. The specificity of these antibodies was examined by competitive ELISA tests using various lignin dimers with different linkages. The anti-dehydrodiconiferyl alcohol antibody reacted specifically with dehydrodiconiferyl alcohol and did not react with other model compounds containing 8-*O*-4′, 8-8′, or 5-5′ linkages. The anti-pinoresinol antibody reacted specifically with pinoresinol and syringaresinol and did not react with the other model compounds containing 8-*O*-4′, 8-5′, or 5-5′ linkages. The antibodies also did not react with dehydrodiconiferyl alcohol acetate or pinoresinol acetate, indicating that the presence of free phenolic or aliphatic hydroxyl group was an important factor in their reactivity. In sections of Japanese cypress (*Chamaecyparis obtusa*), labeling by the anti-dehydrodiconiferyl alcohol antibody was found in the secondary walls of phloem fibers and in the compound middle lamellae, and secondary walls of tracheids. Weak labeling by the anti-pinoresinol antibody was found in secondary walls of phloem fibers and secondary walls and compound middle lamellae of developed tracheids. These labelings show the localization of 8-5′ and 8-8′ linked structure of lignin in the cell walls.

Keywords *Chamaecyparis* · Lignin · Monoclonal antibody · Wood cell wall · 8-5′ linkage · 8-8′ linkage

Abbreviations

BSA	Bovine serum albumin
*p*AHA	*p*-Aminohippuric acid
ELISA	Enzyme-linked immunosorbent assay
MALDI-TOF	MS Matrix-assisted laser desorption/ ionization time-of-flight mass spectrometry
PBS	Phosphate buffered saline
TBS	Tris(hydroxymethyl) aminomethane buffered saline
TEM	Transmission electron microscopy

S. Kiyoto · A. Yoshinaga (✉) · N. Tanaka · M. Wada · K. Takabe
Laboratory of Tree Cell Biology, Division of Forest and Biomaterials Science, Graduate School of Agriculture, Kyoto University, Sakyo-ku, Kyoto 606-8502, Japan
e-mail: aryosshy@kais.kyoto-u.ac.jp

H. Kamitakahara
Laboratory of the Chemistry of Biomaterials, Division of Forest and Biomaterials Science, Graduate School of Agriculture, Kyoto University, Sakyo-ku, Kyoto 606-8502, Japan

Introduction

Lignin is a complex dehydrogenative polymer of monolignols, namely *p*-coumaryl, coniferyl, and sinapyl alcohols. Monolignols are synthesised via complex phenylpropanoid pathway and then polymerized by radical coupling to form

different interunit linkages (Davin et al. 2008). In plant cell walls, lignin, and hemicellulose act as a matrix around cellulose microfibrils. Lignification allows plant cell walls to be more hydrophobic, higher pressure-resistant, and more decay-resistant against microorganisms. Better understanding of the complex structure of lignin is also important to produce various value-added chemicals from biomass.

The proportion of lignin that exhibits condensed structures is an important factor for the reactivity of lignin because condensed structures are resistant to chemical degradation methods such as nitrobenzene oxidation and thioacidolysis. The proportion of the condensed structures of lignin is also important during pulping process. Analysis of dimer compounds derived during thioacidolysis (Lapierre et al. 1991) provides useful information about the proportion of protolignin that exhibits various linkages. However, the yield of these dimeric compounds is not high, and it is difficult to examine their distribution in plant cell walls. Probes that selectively react with specific structures of lignin in situ are useful for determining the localization of condensed structures in lignin polymer and for investigating the processes by which these structures are formed in plant cell walls.

To date, various immunological probes of lignin have been developed. Polyclonal antibodies were raised against various kinds of dehydrogenation polymer (DHP) (Ruel et al. 1994, 1999, 2001; Joseleau and Ruel 1997; Joseleau et al. 2004a, b), milled wood lignin (MWL) (Kim and Koh 1996, 1997), and dibenzodioxocin lignin substructures (Kukkola et al. 2003, 2004).

Monoclonal antibodies have been developed against non-lignin components of the plant cell wall, including pectin (Willats et al. 2006, and references therein, Ralet et al. 2010), xyloglucan (Puhlmann et al. 1994), xylan and arabinoxylan (McCartney et al. 2005), feruloylated-(1-4)-beta-D-galactan (Clausen et al. 2004), *p*-coumarate (Tranquet et al. 2009), and tea polyphenols (Gani et al. 1998). Although the reactivity is more easily affected by the modification of epitope as compared with polyclonal antibodies, these monoclonal antibodies are valuable for the analysis of more highly defined structures in the plant cell wall than polyclonal antibodies since these are composed of one type of immunoglobulin.

Since lignin also contains very complex structures, highly defined monoclonal antibodies against lignin substructures would be effective tools to clarify the mechanism of lignification in the plant cell wall. The antibodies would give us new information that cannot be obtained by other chemical degradation analyses. Jouanin et al. (2000) analyzed dimeric compounds after thioacidolysis and showed that the proportion of 8-5′ dimers was relatively high both in poplar and pine and also that of 8-8′ dimers was relatively high in poplar among other dimeric compounds. This result suggests that the proportion of 8-5′ and 8-8′ linkage is relatively high among various linkages of lignin. Also the proportion of 8-5′ dimers and 8-8′ dimers on the way of polymerization was reported to be relatively high in methanol extracts from lignifying poplar xylem (Morreel et al. 2004). Thus, we prepared monoclonal antibodies directed against dehydrodiconiferyl alcohol- or pinoresinol-*p*-aminohippuric acid-(*p*AHA)-bovine serum albumin (BSA) conjugate. Here we report on the characterization of these monoclonal antibodies that react specifically with 8-5′ or 8-8′ linked structure of lignin in cell walls of *Chamaecyparis obtusa*.

Materials and methods

Preparation of dehydrodiconiferyl alcohol- or pinoresinol-*p*AHA–BSA conjugate

Dehydrodiconiferyl alcohol was a gift from Professor Emeritus Noritsugu Terashima of Nagoya University, Japan. Pinoresinol was synthesised from coniferyl alcohol according to the procedure reported by Quideau and Ralph (1994). The purity of pinoresinol and dehydrodiconiferyl alcohol was confirmed by thin layer chromatography (eluent, dichloromethane:methanol, 95:5, v/v). Dehydrodiconiferyl alcohol or pinoresinol or guaiacylglycerol-beta-guaiacyl ether was diazo-coupled to BSA via *p*AHA, according to the method of Nagasaki et al. (2001) with slight modification. BSA (600 mg) and *p*AHA (60 mg for dehydrodiconiferyl alcohol and 600 mg for pinoresinol and guaiacylglycerol-beta-guaiacyl ether) were dissolved in 360 ml of water and adjusted to pH 8.0 with 1 M NaOH. 1-ethyl-3-(dimethylaminopropyl)-carbodiimide (EDC) (600 mg for dehydrodiconiferyl alcohol and guaiacylglycerol-beta-guaiacyl ether, and 1200 mg for pinoresinol) was added and the pH adjusted to 6.4 with 2 M HCl. The solutions were stirred in the dark at room temperature for 12 h (dehydrodiconiferyl alcohol) or 6 h (pinoresinol and guaiacylglycerol-beta-guaiacyl ether). For pinoresinol and guaiacylglycerol-beta-guaiacyl ether, an additional 300 mg of EDC was added and the stirring continued in the dark at room temperature for an additional 24 h. The reaction mixtures were then dialyzed against sodium phosphate buffer (0.1 M, pH 6.4) and then water. After removal of a small amount of precipitate by centrifugation, the solutions were lyophilized to obtain the *p*AHA–BSA conjugates.

The *p*AHA–BSA conjugates (120 mg for dehydrodiconiferyl alcohol, 25 mg for pinoresinol, 60 mg for guaiacylglycerol-beta-guaiacyl ether) were dissolved in water (20 ml for dehydrodiconiferyl alcohol and guaiacylglycerol-beta-guaiacyl ether, 10 ml for pinoresinol) and adjusted to pH 1.5. The solutions were cooled in an ice

bath, and a few drops of 1 % $NaNO_2$ aqueous solution were added. To remove the excess $NaNO_2$, an aqueous 2 % ammonium sulfamate solution was added until KI starch test paper did not turn blue.

Dehydrodiconiferyl alcohol (20 mg) or pinoresinol (6 mg) or guaiacylglycerol-beta-guaiacyl ether (25 mg) was dissolved in 0.5 ml of methanol and then mixed with pH 9.0 sodium borate buffer (10 ml for dehydrodiconiferyl alcohol and guaiacylglycerol-beta-guaiacyl ether, 5 ml for pinoresinol). This solution was added dropwise to the *p*AHA–BSA conjugate solutions in an ice bath and allowed to react for 30 min. The reaction mixture was dialyzed against sodium borate buffer (pH 9.0) and then water, and finally lyophilized. These conjugates were used for the immunoassays. Guaiacylglycerol-beta-guaiacyl ether-*p*AHA–BSA conjugate was used for screening of hybridoma.

Matrix-assisted laser desorption/ionization time-of-flight mass spectrometry (MALDI-TOF MS)

The amount of *p*AHA in the *p*AHA–BSA conjugates and the amounts of dehydrodiconiferyl alcohol, pinoresinol, and guaiacylglycerol-beta-guaiacyl ether in their respective conjugates were evaluated by MALDI-TOF MS (Bruker Daltonics Reflex III) with sinapic acid as a matrix. For ionization, a nitrogen laser was used. All spectra were measured in the positive linear ion mode using external calibration.

Immunization, hybridoma preparation, and antibody selection

Immunization, hybridoma preparation, and antibody selection were performed by Kohjin Bio, Ltd. (Saitama, Japan) as follows: Four female BALB/c mice were immunized subcutaneously with an emulsion of dehydrodiconiferyl alcohol- or pinoresinol-*p*AHA–BSA conjugate and Freund's complete adjuvant on day 0. On days 14 and 22 the injections of the conjugate were repeated in a similar manner using Freund's incomplete adjuvant. The spleen was removed on day 25. Lymphocytes were isolated and fused with the P3U1 mouse myeloma cell line using polyethylene glycol (PEG) hybridoma preparation and limiting dilution cloning procedures. Hybridoma supernatants resulting from the fusion were screened for the presence of antibodies by enzyme-linked immunosorbent assay (ELISA) using dehydrodiconiferyl alcohol- or pinoresinol-*p*AHA–BSA conjugates as the antigens. A number of cell lines that produce antibody reacted positively with the dehydrodiconiferyl alcohol- or pinoresinol-*p*AHA–BSA conjugates and reacted negatively with the guaiacylglycerol-beta-guaiacyl ether-*p*AHA–BSA conjugate. These lines were selected from the primary screenings for further cloning. After cloning, two monoclonal antibodies (KM1, immunoglobulin subclass IgG1 for dehydrodiconiferyl alcohol and KM2, immunoglobulin subclass IgG2b for pinoresinol) were selected for further characterization.

Immunoassay

To optimize the concentration of antigen and antibody for competitive ELISA tests, ELISA was performed in 96-well microtiter plates (Falcon35–3912) coated with 50 µl of dehydrodiconiferyl alcohol- or pinoresinol-*p*AHA–BSA conjugate per well (10^{-6}–10^{3} µg/ml) and phosphate-buffered saline (PBS) in a tenfold dilution series. The plates were incubated overnight at 4 °C. Unbound antigen was then washed out of the wells thrice with 200 µl of blocking solution (0.3 % skim milk in PBS), and the plates were kept at room temperature with various proteins in skim milk, to block non-specific binding sites of antibody. After 30 min at room temperature, 40 µl of hybridoma supernatant in blocking solution was added per well at the appropriate dilution. After incubation for 1 h at 35 °C, the plates were washed with PBS containing 0.05 % Tween 20 (PBS-T). Then, 40 µl of peroxidase-conjugated goat-anti-mouse IgG, IgA, IgM antibody (ICN/CAPEL) was added per well at a dilution of 1:500. After another 1 h incubation at 35 °C, the plates were washed again with PBS-T. Antibody binding was detected by addition of 50 µl of peroxidase substrate (0.05 M citrate, 0.1 M sodium phosphate buffer pH 5, 0.1 % *o*–phenylendiamine, 0.006 % hydrogen peroxide) per well. The reaction was stopped by addition of 25 µl of 0.2 M sulfuric acid per well, and the absorbance was measured at 492 nm on a microplate reader (MTP-300; Corona Electric, Ibaraki-ken, Japan).

Specificity of the antibodies was then examined by competitive ELISA tests using lignin model compounds containing various lignin substructures (Fig. 1). In native lignin, several dimeric substructures, that is, 8-aryl ether (8-*O*-4′), resinol (8-8′), phenylcoumaran (8-5′), dibenzodioxocin, biphenyl ether (5-*O*-4′), biphenyl (5-5′), and diarylpropane (8-1′) are considered to be dominant (Davin et al. 2008). Dimers that have these substructures except dibenzodioxocin, 5-*O*-4′ and 8-1′ substructures were selected for characterization. Guaiacylglycerol-beta-guaiacyl ether was purchased from Tokyo Chemical Industry Co. Ltd (Tokyo, Japan; purity was 97.0 %, GC). Dehydrodidihydroeugenol with 5-5′ linkage was synthesised from 4-propylguaiacol according to a published method (Pew 1963). Dehydrodiconiferyl alcohol and dehydrodiisoeugenol were gifts from Professor Emeritus Noritsugu Terashima. The microtiter plates (Falcon 35-3912) were again coated with 50 µl per well of dehydrodiconiferyl alcohol- or pinoresinol-*p*AHA–BSA conjugate (100 µg/ml, optimized

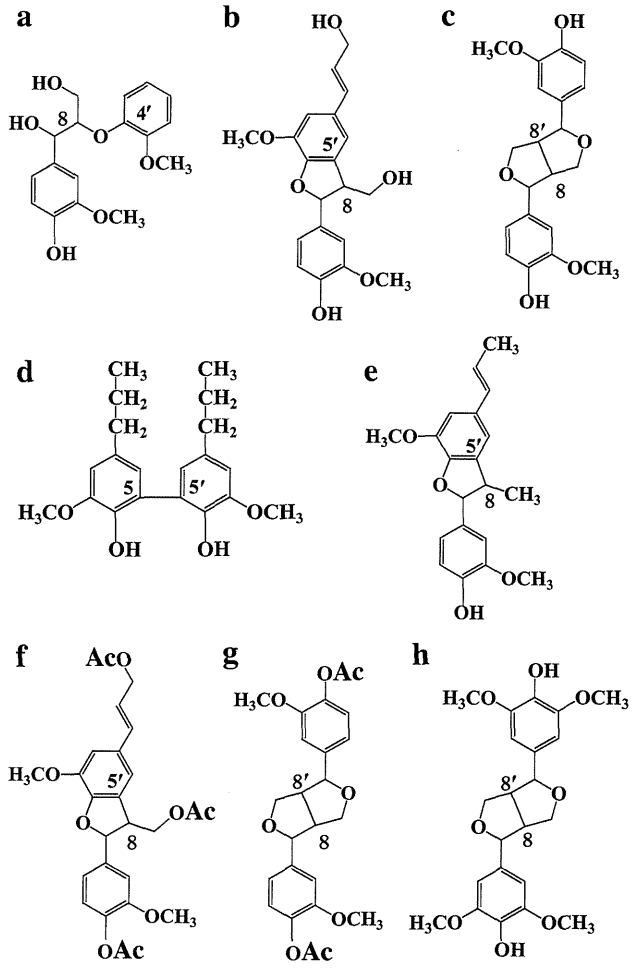

Fig. 1 Lignin model compounds used for competitive ELISA tests of the KM1 and KM2 antibodies. **a** Guaiacylglycerol-beta-guaiacyl ether (8-*O*-4′). **b** Dehydrodiconiferyl alcohol (8–5′). **c** Pinoresinol (8-8′G). **d** Dehydrodidihydroeugenol (5-5′). **e** Dehydrodiisoeugenol (8–5′CH_3). **f** Dehydrodiconiferyl alcohol acetate (8-5′ acetate). **g** Pinoresinol acetate (8-8′ acetate). **h** Syringaresinol (8-8′ S)

concentration) in PBS and incubated overnight at 4 °C. Unbound antigen was then washed out of the wells thrice with 200 µl of blocking solution, and the plates were kept at room temperature to avoid non-specific binding of antibody. The hybridoma supernatant was diluted 1:3 (for the dehydrodiconiferyl alcohol-*p*AHA–BSA conjugate) or 1:300 (for the pinoresinol-*p*AHA–BSA conjugate) with blocking solution and mixed with a lignin model compound that was dissolved in methanol. The final concentration of methanol in the mixture was 10 %. The mixture was incubated at 35 °C for 2 h, after which 40 µl of the mixture per well was added to the plates, and the plates were incubated for 1 h at 35 °C. The plates were then washed with PBS-T, and antibody binding was detected as described above. The absorbance values from controls containing no lignin compound but the same concentration of methanol were taken to indicate 0 % inhibition of antibody binding. The absorbance values from controls with no added antibody were taken to indicate 100 % inhibition of binding.

Plant materials and their preparations for immuno-microscopy

Two trees of Hinoki (Japanese cypress, *C. obtusa*) were cut at Kitashirakawa Experimental Station in the Field Science Education and Research Center of Kyoto University at the beginning of July 2006 (tree 1, 34 years old, height 10.9 m, diameter at breast height 19.7 cm) and at the middle of June 2009 (tree 2, 21 years old, height 7.6 m, diameter at breast height 6.4 cm). Small blocks containing secondary phloem, cambial zone, differentiating xylem produced in current year, and a part of developed xylem produced in previous year were collected from outermost parts of the stem at breast height. They were either fixed with 3 % glutaraldehyde (tree 1) or stored in 70 % ethanol (tree 2) and then dehydrated through an ethanol series and embedded in epoxy resin or LR White resin. Specimens from tree 2 were stored in 70 % ethanol for several weeks, then dehydrated through ethanol series to 99.5 % ethanol, stored for almost 1 year, then washed repeatedly with ethanol before embedding to remove free dimers and minimize the effect of these dimers on immunolabeling. Formation of S_1 and S_3 layers was observed with thin sections (2–3 µm thick) under a polarizing light microscope. Immunogold silver staining for light microscopy.

For light microscopy, immunogold silver staining was performed on 1-µm-thick sections from the embedded blocks. Sections were mounted on MAS-coated glass slides (Matsunami Glass Ind. Ltd., Kishiwada City, Japan) and stained as follows: Sections were incubated for 1 h with 50 mM glycine in PBS at room temperature. After washing with PBS-T, they were incubated with 5 % skim milk in PBS for 2 h at room temperature to avoid non-specific binding of antibody. The sections were then washed with PBS-T and incubated with hybridoma supernatant with 1:10, 1:5, and no dilution or 1 % ascites fluid in 5 % skim milk in PBS overnight at 4 °C. After washing with PBS-T, the sections were incubated at room temperature for 2 h with AuroProbe GAM [1 nm colloidal gold-conjugated goat anti-mouse IgG (H+L), Amersham Biosciences] diluted 1:50 in 5 % skim milk in PBS. They were again washed with PBS-T, fixed with 2 % glutaraldehyde in PBS for 5 min at room temperature, and washed with deionized water. To detect the label, the IntenSE M silver enhancement kit (Amersham Biosciences) was used. The reaction was stopped by washing with deionized water. The sections were then stained with aqueous 0.002 % Azure II methylene blue solution containing sodium tetraborate for 5 min at room temperature, washed with water, dried, and mounted with Canada balsam (Merck, Darmstadt, Germany).

Immunogold labeling for transmission electron microscopy

For transmission electron microscopy, ultrathin sections were cut from the embedded blocks and mounted on nickel grids (200 mesh). The sections were soaked in a drop of blocking buffer (1 % BSA, 0.1 % NaN_3, 0.1 % Tween20 in TBS) for 30 min at room temperature. The sections were then soaked in a drop of hybridoma supernatant for 2 days at 4 °C. The sections were washed three times for 15 min each in several drops of blocking buffer and then incubated at 35 °C for 2 h with 1 % goat anti-mouse secondary antibody labeled with 10 nm colloidal gold particles (EMGAM10; BBInternational, Cardiff, UK) in blocking buffer. Finally, the sections were washed six times for 15 min each in several drops of blocking buffer and then washed with deionized water. The sections were observed under a transmission electron microscope (JEM1400, JEOL, Japan) at 80 or 100 kV.

Results

Evaluation of antigens by MALDI-TOF MS

Figure 2 shows the MALDI-TOF MS spectra of BSA, *p*AHA–BSA, and the dehydrodiconiferyl alcohol-*p*AHA–BSA, pinoresinol-*p*AHA–BSA, and guaiacylglycerol-beta-guaiacyl ether-*p*AHA–BSA conjugates. The molecular weights of the conjugates, estimated from the spectra, were approximately 6.7×10^4 (BSA, Fig. 2a), 7.2×10^4 (*p*AHA–BSA, Fig. 2b), 7.3×10^4 (dehydrodiconiferyl alcohol-*p*AHA–BSA, Fig. 2c), 7.5×10^4 (*p*AHA–BSA, Fig. 2d), 7.8×10^4 (pinoresinol-*p*AHA–BSA, Fig.2e), 7.4×10^4 (*p*AHA–BSA, Fig. 2f), and 7.5×10^4 (guaiacylglycerol-beta-guaiacyl ether-*p*AHA–BSA) (Fig. 2g). The difference in molecular weight of three *p*AHA was due to the different conditions used for preparation. Comparing the molecular weights of the conjugates with those of corresponding *p*AHA–BSA permitted a rough estimate of the number of covalently bonded lignin model compounds, namely dehydrodiconiferyl alcohol, pinoresinol, and guaiacylglycerol-beta-guaiacyl ether, in their *p*AHA–BSA conjugates; the numbers were 3, 10, and 5 (mol/mol), respectively. According to Erlanger (1980), epitope density affects an antibody titer to the hapten. A more precise evaluation of the number of covalently bonded molecules on the *p*AHA–BSA was not possible because the peaks of the MALDI-TOF MS spectra were broad. However, the conjugation of lignin model compounds to BSA was confirmed from the peak shifts.

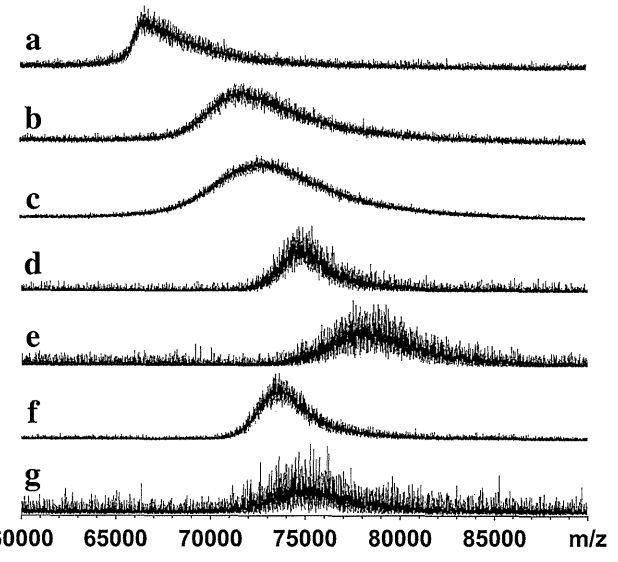

Fig. 2 MALDI-TOF MS spectra of various conjugates used for producing antibody and its characterization. **a** BSA. **b** *p*AHA–BSA conjugate. **c** Dehydrodiconiferyl alcohol-*p*AHA–BSA conjugate synthesised from **b**. **d** *p*AHA–BSA conjugate. **e** Pinoresinol-*p*AHA–BSA conjugate synthesised from **d**. **f** *p*AHA–BSA conjugate. **g** Guiacylglycerol-beta-guaiacyl ether-*p*AHA–BSA conjugate synthesised from **f**

Isolation of a mouse monoclonal antibody

Immunization with dehydrodiconiferyl alcohol- or pinoresinol-*p*AHA–BSA conjugates was effective in inducing an immune response against dehydrodiconiferyl alcohol or pinoresinol. ELISA-based primary screening with the dehydrodiconiferyl alcohol- or pinoresinol-*p*AHA–BSA conjugates, *p*AHA–BSA conjugate, and guaiacylglycerol-beta-guaiacyl ether-*p*AHA–BSA conjugate identified ten positive antibody-secreting cell lines for dehydrodiconiferyl alcohol and 12 cell lines for pinoresinol. These lines showed a positive reaction against dehydrodiconiferyl alcohol- or pinoresinol-*p*AHA–BSA conjugate. Eight lines for dehydrodiconiferyl alcohol and eight lines for pinoresinol were finally cloned. Among these lines, the lines that showed a positive reaction against dehydrodiconiferyl alcohol- or pinoresinol-*p*AHA–BSA conjugate and a negative reaction against the guaiacylglycerol-beta-guaiacyl ether-*p*AHA–BSA conjugate and *p*AHA–BSA were selected. In preliminary observations using immunogold silver staining of wood sections with these cell lines, the three lines for dehydrodiconiferyl alcohol gave positive immunogold silver staining of cell wall and one line which gave strongest staining was selected (KM1, immunoglobulin subclass IgG1). For pinoresinol, four lines gave positive immunogold silver staining of cell wall and one line which gave strongest staining was selected (KM2, immunoglobulin subclass